Annu. Rev. Nucl. Part. Sci. 2002. 52:339–96
doi: 10.1146/annurev.nucl.52.050102.090637

EFFECTIVE FIELD THEORY FOR FEW-NUCLEON SYSTEMS*

Paulo F. Bedaque
Nuclear Science Division, Lawrence Berkeley National Laboratory, One Cyclotron Road, Berkeley, California 94720; e-mail: pfbedaque@lbl.gov

Ubirajara van Kolck
Department of Physics, University of Arizona, Tucson, Arizona 85721; e-mail: vankolck@physics.arizona.edu; RIKEN BNL Research Center, Brookhaven National Laboratory, Upton, New York 11973

Key Words chiral perturbation theory, nuclear physics, few-body systems

PACS Codes 11.10.−z, 21.30.−x, 21.45.+v

■ **Abstract** We review the effective field theories (EFTs) developed for few-nucleon systems. These EFTs are controlled expansions in momenta, where certain (leading-order) interactions are summed to all orders. At low energies, an EFT with only contact interactions allows a detailed analysis of renormalization in a nonperturbative context and uncovers novel asymptotic behavior. Manifestly model-independent calculations can be carried out to high orders, leading to high precision. At higher energies, an EFT that includes pion fields justifies and extends the traditional framework of phenomenological potentials. The correct treatment of QCD symmetries ensures a connection with lattice QCD. Several tests and prospects of these EFTs are discussed.

CONTENTS

1. INTRODUCTION

1.1. Why Effective Theories?

Nuclear systems have often been described as pathologically complicated. The forces between the constituent nucleons are strong and noncentral, and the relatively small binding found in nuclei results from detailed cancellations between much larger contributions. Given our incomplete knowledge of the basic interaction among nucleons, especially at short distances, and the problems involved in the numerical solution of the Schrödinger equation for systems with many fermions, one can understand why nuclear structure remains an unsolved problem after decades of intense effort. This seems even more frustrating when one remembers that all nuclear processes are encoded in the QCD Lagrangian and that parameter-free predictions could, in principle, be obtained.

Despite all the difficulties, enormous progress has been made throughout the years by the use of models that capture different aspects of nuclear phenomena. One dissatisfying aspect of these models, however, is their ad hoc nature and the presence of uncontrolled approximations. These models are not derived from any basic principle (and certainly not from QCD) and contain information that comes from decades of trial and error hidden behind apparently arbitrary choices of some contributions over others. Each new improvement involves the same process of educated guesses, and one is never sure what a reasonable error estimate would be. Effective field theories (EFTs) are useful because they provide a systematic expansion in a small parameter that organizes and extends previous phenomenological knowledge about nuclear processes, and they provide a rigorous connection to QCD. They also help with more technical but important issues that have plagued nuclear physics in the past, including gauge invariance, "off-shell" effects, and relativistic corrections, by borrowing heavily from the arsenal of field theory.

1.2. What is an Effective Theory?

Most of the uncertainty in nuclear processes comes from the short-distance interactions ($\lesssim$1 fm) between two or more nucleons (and photons, leptons). Even when one is interested only in low-energy phenomena, the short-distance contributions can be important. In perturbation theory, for instance, the influence of short-distance physics on low-energy observables is manifested by ultraviolet-divergent integrals, that is, by the dominance of high-momentum modes over low-momentum ones.

Sensitivity of large-distance observables to short-distance physics is not unusual; it is, in fact, pervasive in many fields of physics. One way of dealing with it is to model the short-distance physics and solve the problem by using a microscopic approach. In the case of nuclear systems, this would lead either to a calculation of nuclear processes directly from QCD (which is currently impossible and would be, even if possible, highly inefficient), or by recourse to meson-exchange or quark or skyrmion models. Another approach is the use of effective theories (1).[1] Before introducing the particular case used in nuclear physics, let us consider effective theories in general.

Suppose we want to study the low-energy behavior of a system described by some theory that we will call the "fundamental" theory. In the path-integral formalism, we can imagine integrating over the high-momentum modes $k > \Lambda$, where the scale Λ is chosen to be much larger than the momentum scale we want to study. The result of this partial integration over the high-momentum modes will be a complicated Lagrangian containing an infinite number of terms. This Lagrangian, called the effective Lagrangian, will generally be nonlocal, but this nonlocality, arising from the momenta $k > \Lambda$, will be restricted to a spatial scale $\lesssim 1/\Lambda$. One can thus expand those interaction terms in a Taylor series in powers of ∂/Λ, where ∂ stands for a derivative of the fields. The coefficients of this expansion do not depend on the soft momenta carried by the fields of the effective theory and describe the hard physics within the scale $1/\Lambda$. They are, however, functions of Λ (the coupling constants "run"). The soft ($k < \Lambda$) and hard ($k > \Lambda$) physics is factorized in the effective Lagrangian. These effective-Lagrangian coefficients are usually called low-energy constants (LECs), since they encode all we need to know about the fundamental theory in order to compute low-energy observables. Notice that, up to this point, no approximation was made and the effective Lagrangian contains exactly the same information as the fundamental one. Calculations of observables done using the effective Lagrangian will contain two sources of Λ dependence. One is the implicit dependence contained in LECs; the other appears in the cutoff that should be used in those computations. These two sources of Λ dependence, by construction, cancel each other.

What is the advantage in separating the integration over momentum modes in two steps? The answer to this question depends on the situation at hand. In problems where the integration over the high-momentum modes can be explicitly accomplished, the effective Lagrangian is a bookkeeping device that allows us to perform approximations in a very efficient way. Examples include nonrelativistic QED (2), heavy-quark effective theory (3), and high-density QCD chiral perturbation theory (4). In other cases, such as the nuclear systems considered here, we will not be able to explicitly integrate the high-momentum modes. We can,

[1]The term "effective theories" has other meanings besides the one articulated in this review. "Effective Lagrangian" sometimes means the Lagrangian that includes all quantum corrections. Other times "effective theory" refers to any model useful at low energies, whether or not there is a separation of scales and a rigorous expansion in powers of the momentum.

however, determine the effective Lagrangian by a combination of self-consistency requirements and experimental data.

We start by considering the most general Lagrangian that is consistent with the symmetries of the underlying theory. This Lagrangian contains an infinite number of arbitrary constants. For a fixed Λ, different values of the LECs describe different underlying theories. Just one set of these values will make our low-energy theory reproduce the same observables as the fundamental theory. We then resort to an approximation scheme: We expand the low-energy observables in powers of the small parameter $Q/\Lambda \ll 1$, where Q is a low-energy scale such as the momenta of the external particles or light masses. Now the factorization between high- and low-momentum contributions comes in handy. Instead of using the full effective Lagrangian, with its infinite number of terms, we can argue that, at a given order in the Q/Λ expansion, only a finite number of terms will contribute, since the remaining terms will include many powers of $\partial/\Lambda \sim Q/\Lambda$. We are left with a much simpler Lagrangian, with a finite (ideally, small) number of coefficients that can be determined from some experimental data (or from the fundamental theory, if possible, or models) and used to predict others. Increasing the order in Q/Λ of a calculation will increase its precision but may also bring other LECs that will have to be determined by experiment.

The argument that connects the order of the expansion in powers of Q/Λ and the terms in the effective Lagrangian that need to be included at that order (called "power counting") varies case by case but always includes two steps. The first step is to estimate the size of diagrams, given the size of the LECs appearing on the vertices, and it is simply done by dimensional-analysis arguments. The second step is to estimate the size of the LECs themselves. We first determine their running, that is, their dependence on Λ, by requiring physical observables to be Λ-independent (at the order in Q/Λ of our approximation). The information about the evolution of the LECs is not by itself enough to determine them, since we do not know their initial conditions. Although for some particular value of Λ one LEC might be passing through zero, this is very unlikely. We assume that a typical size for a LEC $C(\Lambda)$ is $C(\Lambda) \sim C(2\Lambda) - C(\Lambda)$, that is, the LECs should have the same order of magnitude as the size of their running. In perturbative settings, this principle amounts to little more than dimensional analysis and is known as naive dimensional analysis (5). Strictly, this provides only a reasonable lower bound, so one should be aware of possible violations of this principle. This estimate, of course, is used only in arguing that some terms in the effective Lagrangian will have a negligible effect and can be dropped. The values of the LECs actually kept in the calculation are determined by experimental data. Notice that, for a given set of symmetries and low-energy degrees of freedom, there is no guarantee that the effective Lagrangian can be truncated at any order in Q/Λ, that is, there is no guarantee that a consistent power counting can be found.

The version of the EFT method sketched above is sometimes called the Wilsonian effective theory. Another version of the same idea is the "continuum" effective theory (3). The continuum effective theory reproduces the same vertices

and propagators as the full theory at low energy. The two theories differ in the ultraviolet region, but this difference can always be absorbed in the values of the LECs. The continuum effective theory's technical advantage over the Wilsonian approach resides in being able to integrate over all momenta (used in conjunction with dimensional regularization), and not only over $k < \Lambda$. This makes it simpler to maintain gauge, chiral, and spacetime symmetries, and to avoid power-law divergences that sometimes complicate power counting.

1.3. How?

EFTs can be used in a few different ways in nuclear physics. Historically, the first one was to set the separation scale Λ around the ρ-meson mass and keep as low-energy degrees of freedom the pions and the nucleons[2] (and maybe the Δ isobars), as well as photons and leptons (6–11). This approach builds on the success of chiral perturbation theory (χPT) in the mesonic and one-baryon sectors. Like nuclear potential models, it describes nonrelativistic nucleons interacting through a potential, but it also brings ingredients of its own, such as a small expansion parameter, consistency with the chiral symmetry of QCD, and systematic and rigorous ways of including relativistic corrections and meson-exchange currents.

Another application of EFT ideas in nuclear physics is made possible by the existence of shallow bound states, that is, binding energies far below any reasonable QCD scale (12–15). We can then set Λ around the pion mass and keep as low-energy degrees of freedom only the nucleons (and photons and leptons). At least in the case of two- and three-body systems, the bound states will be within the range of validity of this simpler theory. This "pionless" effective theory can be considered as a formalization and extension of the old effective-range theory (ERT) (16) and the work on "model-independent results" in three-body physics (17). The new features, besides the existence of a small parameter on which to expand, appear in a number of new short-distance contributions describing exchange currents and three-body forces, as well as in relativistic corrections, that are transparent in this approach. An extra bonus is the possibility of deriving analytic, high-precision expressions for many observables that previously required nontrivial numerical work.

In Sections 2 and 3, we review these two approaches in few-nucleon systems, emphasizing qualitative aspects of recent developments. In Section 4, we present an outlook, including other approaches that are being developed for larger nuclei. Other reviews have already covered applications of EFT ideas to nuclear physics, with different emphasis from the present one (18). Many developments of the past couple of years are described in Reference (19).

[2]Since energies are measured from the ground state with a given baryon number, slow nucleons, despite carrying large rest-mass energy, should be considered low-energy degrees of freedom.

2. EFFECTIVE FIELD THEORY WITHOUT EXPLICIT PIONS

2.1. The Two-Nucleon System and the Nontrivial Fixed Point

2.1.1. TWO-NUCLEON SCATTERING Let us now apply the ideas outlined in the previous section to the specific case of two nucleons with momentum k below the pion scale $k < m_\pi$ (see Reference (15) for more details). We start by writing the most general Lagrangian that involves only two nucleons (electroweak external currents will be included later). A system with two nucleons with zero angular momentum ($L = 0$) can exist in a spin singlet ($^1S_0$) or spin triplet ($^3S_1$) state so there are two independent interactions with no derivatives,

$$\begin{aligned}\mathcal{L} = N^\dagger\Big(i\partial_0 + \frac{\vec{\nabla}^2}{2M} + \dots\Big)N - C_{0t}\big(N^T P_t N\big)^\dagger\big(N^T P_t N\big) \\ - C_{0s}\big(N^T P_s N\big)^\dagger\big(N^T P_s N\big) + \dots,\end{aligned} \tag{1.}$$

where

$$\begin{aligned}P_t^i &= \frac{1}{\sqrt{8}}\sigma_2\sigma^i\tau_2, \\ P_s^A &= \frac{1}{\sqrt{8}}\tau_2\tau^A\sigma_2\end{aligned} \tag{2.}$$

are the projectors in the triplet and singlet spin-isospin states (σs act on spin space, τs on isospin space), M is the nucleon mass, and N is the nucleon field. The dots in Equation 1 stand for terms with more derivatives that, as we argue below, will be subdominant.

The nucleon-nucleon (NN) scattering amplitude can be written in terms of the phase shift δ as

$$\begin{aligned}T &= \frac{4\pi}{M}\frac{1}{k\cot\delta - ik} \\ &= \frac{4\pi}{M}\frac{1}{-\frac{1}{a_s} + \frac{r_{0s}}{2}k^2 + \dots - ik}.\end{aligned} \tag{3.}$$

It can be shown that, for potentials of range $\sim R$ ($R \sim 1/m_\pi$ in our case), $k\cot\delta$ is an analytic function around $k = 0$ and has a cut starting at $k^2 \sim 1/R^2$, so it is well approximated by a power series as shown in the last line of Equation 3. The parameter a_s (r_{0s}) is called the singlet scattering length (singlet effective range). For notational simplicity, we focus for now on the spin singlet channel.

Figure 1 shows the graphs that contribute to NN scattering generated by the Lagrangian in Equation 1. The L-loop graph factorizes into a power,

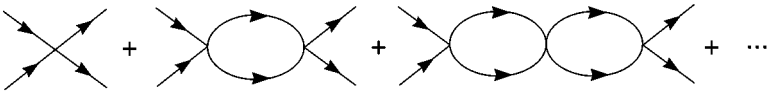

Figure 1 Graphs contributing to the leading-order *NN* scattering amplitude.

$$L\text{-loop graph} \sim (c\Lambda - ik)^L, \qquad 4.$$

each one containing a linearly divergent piece and the unitarity cut ik (in the center-of-mass system with total energy k^2/M). The loop integral is linearly divergent and the coefficient c is dependent on the particular form of the regulator used, that is, the particular form by which the high-momentum modes are separated from the low-momentum ones. Using a sharp momentum cutoff, for instance, we have $c = 2/\pi$, using dimensional regularization, $c = 0$. The sum of all graphs in Figure 1 is a geometrical sum that gives

$$T = \frac{4\pi}{M} \frac{1}{-\frac{4\pi}{MC_{0s}} + c\Lambda - ik}. \qquad 5.$$

We see then that terms shown explicitly in Equation 1 reproduce the first term of the effective range expansion. The addition of terms with more derivatives will reproduce further terms in the effective range expansion.

We can learn some important lessons from this simple calculation. Let us consider two separate situations.

- **Natural case:** For a generic potential with range R, the effective-range parameters typically have similar size, $a \sim r_0 \sim R$. Using dimensional regularization, C_0 can be chosen to be $C_0 = 4\pi a/M$ (this choice is called minimal subtraction). The effective theory is valid for $k < 1/R$ and, in this range, T can be expanded as

$$T = \frac{4\pi}{M}\left[-a + ika^2 + \left(\frac{a^2 r_0}{2} + a^3\right)k^2 + \ldots\right]. \qquad 6.$$

  Because $C_0 \sim a$, there is a one-to-one correspondence between the order in the ka expansion, the number of C_{0s} vertices, and the number of loops in a graph. The leading order (LO) is given by one tree-level diagram, the next-to-leading order (NLO) by the one-loop diagram, and next-to-next-to-leading order (N^2LO) by the two-loop diagram involving C_0 and one tree-level diagram with a two-derivative vertex (not shown in Equation 1), and higher orders are treated similarly. We have then a perturbative expansion, even though the microscopic potential can be arbitrarily strong. If one uses a cutoff regulator, the situation is slightly more complicated. Choosing $\Lambda \sim 1/R \sim 1/a$, we note that the most divergent piece of the multi-loop graphs is as large as the tree-level graph and must be resummed to all orders, whereas the energy-dependent part containing powers of ikC_0 is suppressed. The pieces

that need to be resummed at LO merely renormalize the constant C_0. The one-to-one correspondence between the order in the *ka* expansion and the number of loops is lost in any renormalization/regularization scheme except the dimensional regularization with minimal subtraction. The technical advantages arising from the use of dimensional regularization and renormalization theory in this perturbative setting were used in the study of dilute gases with short-range interactions (20).

- **Unnatural case:** In the nuclear case, the scattering lengths of the two *S*-wave channels are much larger than the range of the potential. The ${}^1S_0$ (neutron-proton) scattering length a_s is $a_s = -23.714$ fm and the scattering length of the triplet (deuteron) channel ${}^3S_1$ is $a_t = 5.42$ fm, corresponding to momentum scales of $1/a_s = 8.3$ and $1/a_t = 36$ MeV, respectively. Those scales are much smaller than the pion mass, $m_\pi \simeq 140$ MeV, defining the range of the nuclear potential.[3] Actually, as we will see below, the potential due to pion exchange is too weak to describe the low-energy phase shifts, and the physics corresponding to the large scattering lengths occurs at the QCD scale $M_{\rm QCD} \sim 1$ GeV, which makes the discrepancy between nuclear and QCD scales even more startling. The origin of the fine-tuned cancellations that lead to the disparity between the underlying scale and the *S*-wave scattering lengths (and deuteron binding energy) is presently unknown. It does not appear in any known limit of QCD, such as the chiral limit ($m_q \to 0$) or large number of colors ($N_c \to \infty$). We simply assume that this cancellation happens, track the dependence of observables on the new soft scale $1/a_{s,t}$, and perform our low-energy expansion in powers of $kR \ll 1$ while keeping the full dependence on $ka_{s,t} \sim 1$. The singlet *NN* scattering amplitude, for instance, will be expanded as

$$T = -\frac{4\pi}{M}\left(\frac{a_s}{1+ika_s} + \frac{k^2 a_s^2 r_{0s}}{2}\frac{1}{(1+ika_s)^2} + \ldots\right). \qquad 7.$$

It is challenging to reproduce an expansion of this form in the EFT. If one uses a momentum cutoff, for instance, the chosen constant C_{0s} must be $C_{0s} = (4\pi/M)(1/a_s + c\Lambda)^{-1}$. The one-loop graph is then suppressed compared to the tree-level one by a factor of $\sim MkC_{0s} \sim k/\Lambda$, and one would naively imagine that the LO contribution is given solely by the tree-level graph. But there are cancellations among the graphs in Figure 1, and all these graphs must be taken into account to reproduce the expansion of T above (13, 14). In the *NN* scattering case considered here, it is not difficult to see which graphs must be included at each order, but in more complex situations this can be extremely tricky. A more convenient way to proceed is to use a renormalization prescription that shifts contributions from high-momentum modes to the

[3]Alkali atoms used in cold atomic traps frequently have scattering lengths much larger than their sizes. They can be made even larger by the use of a carefully tuned external magnetic field (Feshbach resonances). All the ideas and formalisms developed to deal with this fact in the nuclear domain have been used to study the physics of atomic traps (21, 22).

LECs in such a way as to eliminate "accidental" cancellations between different diagrams. One can determine which diagrams contribute at each order on a diagram-by-diagram basis (manifest power counting). One way to do that is to use dimensional regularization with a "power divergence subtraction" (23).[4] In this scheme, we add to and subtract from the denominator of the bubble sum in Equation 5 an amount $M\mu/4\pi$, where μ is an arbitrary scale, and absorb the subtracted term in a redefinition of the constant $C_{0s}(\mu)$, which now is a function of μ. We have for the LO amplitude

$$T = -\frac{4\pi}{M}\frac{1}{\frac{4\pi}{MC_{0s}(\mu)} + ik + \mu}. \qquad 8.$$

The constant $C_{0s}(\mu)$ is now chosen to be

$$C_{0s}(\mu) = \frac{4\pi}{M}\frac{1}{\frac{1}{a_s} - \mu}, \qquad 9.$$

in order to reproduce the LO piece of the expansion in Equation 7. The explicit dependence on μ cancels against the implicit dependence contained in $C_{0s}(\mu)$. The point of this rearrangement is that if μ is chosen so that $\mu \sim 1/a_s$, then $C_{0s}(\mu) \sim 4\pi/M\mu$ and the contribution of all diagrams in the bubble sum are of the same order, justifying the need to resum them. Let us see how this works in some detail. If we denote the soft scales $1/a_s$, μ, and k collectively by Q, the tree-level diagram is of the order $C_{0s} \sim 4\pi/MQ$. The one-loop graph contains two powers of C_{0s}, two nucleon propagators (each one counting as $1/(k^2/M) \sim M/Q^2$), and a loop integral with three powers of momentum ($\sim Q^3$), one of energy ($\sim Q^2/M$), and the usual factor of $1/4\pi$ from the loop integration, for a total of $(4\pi/MQ)^2(M/Q^2)^2Q^5/4\pi M \sim 4\pi/MQ$. Thus, the one-loop diagram is the same size as the tree-level graph. The same occurs for the remaining diagrams, and they all have to be resummed. It is interesting to note that this reshuffling of contributions between the divergent loop and the LECs amounts to subtracting the poles $1/(D-2)$ that would exist in $D = 2$ space dimensions. One can easily go to higher orders and include terms with derivatives in the Lagrangian. A simple calculation (again, subtracting the pole that occurs at $D = 2$) leads to expressions for all the LECs in terms of the effective-range parameters (and of the arbitrary scale μ). For instance, if C_{2n} denotes the coefficient of operators with $2n$ derivatives,

$$C_{2s} = \frac{4\pi}{M}\frac{r_{0s}}{2}\left(\frac{1}{\frac{1}{a_s} - \mu}\right)^2, \qquad 10.$$

$$C_{4s} = \frac{4\pi}{M}\left[\frac{r_{0s}^2}{4}\left(\frac{1}{\frac{1}{a_s} - \mu}\right)^3 + \frac{r_{1s}^3}{2}\left(\frac{1}{\frac{1}{a_s} - \mu}\right)^2\right], \qquad 11.$$

[4]Other schemes also solve this problem (24).

where the "shape parameter" r_{1s} is the coefficient of the third term of the effective-range expansion.

The β-function that describes the evolution of the dimensionless coupling $\hat{c}_{0s} \equiv -M\mu C_{0s}/4\pi$ is

$$\mu \frac{\partial}{\partial \mu} \hat{c}_{0s}(\mu) = \hat{c}_{0s}(\mu)\,[1 - \hat{c}_{0s}(\mu)]\,. \qquad 12.$$

Note the existence of two fixed points (23, 25), the trivial (perturbative) one at $\hat{c}_{0s} = 0$ and a nontrivial one at $\hat{c}_{0s} = 1$. For $\mu \ll 1/|a_s|$, as appropriate to the natural case discussed above, $\hat{c}_{0s}$ is close to the trivial fixed point. Diagrams involving more C_{0s} vertices are suppressed by powers of $\hat{c}_{0s} \ll 1$ and the system is perturbative. The value $\hat{c}_{0s} \sim \mu a_s$ corresponds to the naive-dimensional-analysis value and the effects of the C_{0s} operator become smaller at lower energies (the operator is irrelevant). On the other hand, for values of $\mu \sim 1/|a_s|$ or larger, adequate to the fine-tuned case discussed here, the flow is close to the nontrivial fixed point. Since $\hat{c}_{0s} \sim 1$, the addition of more C_{0s} vertices is not suppressed and all graphs containing only this vertex should be resummed. The dimensionless coupling $\hat{c}_{0s}$ goes from the naive-dimensional-analysis value $\hat{c}_{0s} \sim \mu a_s$ to $\hat{c}_{0s} \sim 1$, and its effects do not go away in the infrared (marginal operator).

Because the ${}^3S_1$ scattering length is also unnaturally large (and consequently the deuteron binding is unnaturally shallow), the same power counting used in the singlet channel applies also to the triplet channel. *NN* scattering in this channel is more complicated because nuclear forces, being noncentral, mix it with the ${}^3D_1$ channel. New operators, starting with two derivatives, describe this mixing. Their coefficients are determined from an expansion of the mixing angle analogous to Equation 7. Also, the LECs are usually determined by matching to an effective-range expansion centered on the deuteron pole, rather than on $k = 0$ as in the singlet channel. The ${}^3S_1$ *NN* amplitude is parameterized as

$$T = \frac{4\pi}{M} \frac{1}{-\gamma + \frac{\rho(k^2+\gamma^2)}{2} + \cdots - ik}, \qquad 13.$$

where γ^2/M is the deuteron binding energy and ρ the effective-range parameter. Explicit expressions for the leading terms in the Lagrangian and numerical values for the LECs can be found in Reference (15).

The inclusion of external currents (photons, neutrinos, etc.) is straightforward. All terms involving nucleons and the new fields or currents should be included, as long as they satisfy the symmetries of the underlying theory. In the case of photons, some of these terms are simply required by gauge invariance and are determined by minimally coupling the photon to the nucleon Lagrangian. Their coefficients are thus fixed by *NN* scattering data and gauge invariance. There are also terms that are gauge-invariant by themselves but whose coefficients are not determined by *NN* scattering data alone. They represent the physics of exchange currents, quark effects, etc., and must be determined through some extra piece of

experimental data. To perform the low-energy expansion, though, it is necessary to have an a priori estimate of the size of these added terms. This estimate is obtained by using the fact that observables should be independent of the cutoff (or μ if one is using dimensional regularization), at least up to the order one is computing.

Consider some two-nucleon (NN) operator of the form $X = C_{2n}^X N^\dagger N^\dagger \Gamma_X \vec{\partial}^{2n} NN$, where Γ_X is some tensor in spin-isospin space. Its matrix element on NN states is given by the diagrams involving the operator X "sandwiched" between two NN scattering amplitudes and by one-loop one-body diagrams that do not involve X. Typically, the one-body diagram is not divergent and does not introduce any μ dependence,[5] so the remaining graphs must be μ-independent by themselves. We have to make a distinction now between the cases where the operator X connects two S-wave states, two non–S-wave states, or one S-wave and one non–S-wave state. In the first case, renormalization-group invariance of the NN matrix element of X implies

$$\mu \frac{\partial}{\partial \mu} C_{2n}^X(\mu) \left(\frac{T}{C_0(\mu)} \right)^2 = 0, \tag{14.}$$

where T is the LO NN scattering matrix, which is μ-independent. It then follows that $C_{2n}^X(\mu)$ scales as $\sim(\mu - 1/a)^{-2}$. Similarly, for the case where X connects one S-wave or no S-wave states, $C_{2n}^X(\mu)$ scales as $\sim(\mu - 1/a)^{-1}$ or $\sim(\mu - 1/a)^0$, respectively. Using dimensional analysis to fix the powers of Λ, we then have

$$C_{2n}^X(\mu) \sim \frac{1}{M(1/a - \mu)^\alpha} \frac{1}{\Lambda^{2n+1-\alpha}}, \tag{15.}$$

where α is the number of S-wave states the operator X can connect (either 0, 1 or 2).

In a nutshell, the power counting rules valid for the NN system are (13–15, 23):

$$\begin{aligned} \text{fermion line} &\to M/Q^2 \\ \text{loop} &\to \frac{Q^5}{4\pi M} \\ \vec{\partial} &\to Q \\ \partial_0 &\to Q^2/M \\ C_{2n} &\to \frac{4\pi}{M\Lambda^n Q^{n+1}} \\ C_{2n}^X &\to \frac{4\pi}{M\Lambda^{2n+1-\alpha} Q^\alpha}, \end{aligned} \tag{16.}$$

[5]One exception is the NN, no-external-current C_4 operator, whose renormalization is driven by C_2. This explains the apparent discrepancy between Equation 10 and Equation 15.

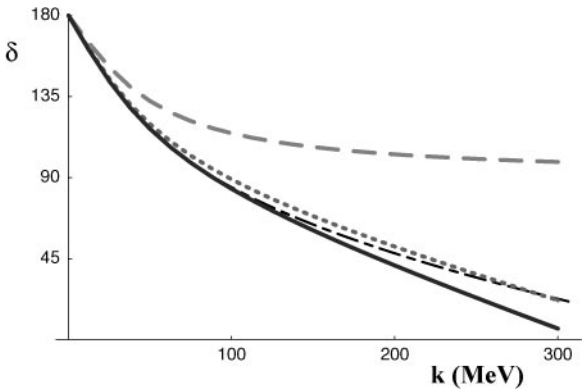

Figure 2 ${}^3S_1$ *NN* phase shift (in degrees) as function of the center-of-mass momentum. The LO result is the dashed line, the N^{2}LO is the dotted line, and N^{4}LO is the solid curve. The dot-dashed line is the Nijmegen phase-shift analysis. (From Reference (15), courtesy of M. Savage.)

where C_{2n} is the coefficient of the *NN* interaction with *2n* derivatives, C_{2n}^X is the coefficient of a *NN* operator with external current *X* and *2n* derivatives, and Λ is the high-energy scale $\Lambda \sim m_\pi$.

Using this rule, we can determine the contributions to *NN* scattering at any given order. At LO, for instance, we have the series of diagrams shown in Figure 1, with all the vertices containing no derivative. That is the only nonperturbative resummation necessary. At NLO, we have the insertion of one C_2 operator in a chain of C_0 operators. At N^{2}LO, we have two insertions of C_2 and one insertion of C_4, and so on. As an example, Figure 2 shows the resulting ${}^3S_1$ phase shift and compares it to the Nijmegen phase-shift analysis (26). Analytic expressions for the phase shifts (see Reference 15) suggest convergence for momenta $k \lesssim 100$ MeV, which is reasonable for an EFT without explicit pions. Electromagnetic effects in proton-proton scattering were considered in the EFT approach in Reference (27).

Up to this point, we have considered only *NN* scattering, where the predictive power of the pionless EFT is very small. We were able, however, to determine many LECs using scattering data and understand the effects of the fine-tuning on the *S*-wave channels. We now apply the formalism developed above to the computation of form factors and processes that involve external currents. We omit the diagrams that need be computed and the explicit analytic expressions that are always available in the *NN* sector. They can be found in the literature cited.

2.1.2. ELECTROMAGNETIC FORM FACTORS OF THE DEUTERON The matrix element of the electromagnetic current on the deuteron has the nonrelativistic parameterization

$$\langle p', \epsilon^j | J^0_{\rm em} | p, \epsilon^i \rangle = e \left[F_C(q^2)\delta_{ij} + \frac{1}{2M_d^2} F_Q(q^2) \left(q_i q_j - \frac{1}{3} q^2 \delta_{ij} \right) \right] \left(\frac{E + E'}{2M_d} \right),$$

$$\langle p', \epsilon^j | \vec{J}^k_{\rm em} | p, \epsilon^i \rangle = \frac{e}{2M_d} \Bigg[F_C(q^2)\delta_{ij}(p + p')^k + F_M(q^2) \left(\delta^k_j q_i - \delta^k_i q_j \right) + \frac{1}{2M_d^2} F_Q(q^2) \left(q_i q_j - \frac{1}{3} q^2 \delta_{ij} \right) (p + p')^k \Bigg], \quad 17.$$

where $|p, \epsilon^i\rangle$ is the deuteron state with momentum p and polarization ϵ^i, M_d is the deuteron mass, $q = p' - p$, and the form factors are normalized such that $F_C(0) = 1$ (deuteron charge), $eF_M(0)/2M_d = \mu_D$ (deuteron magnetic moment), and $F_Q(0)/M_d^2 = \mu_Q$ (deuteron quadrupole moment).

At LO and NLO, the computation of $F_C(q^2)$ involves only the constants C_{0t} and C_{2t} and is identical to the ERT calculation. At N^{2}LO, a one-body term describing the nucleon mean-square charge radius ($\langle r^2 \rangle_N$) appears, which is the first deviation from ERT (15). Formally, there are also relativistic corrections, but they are suppressed by powers of Q/M as opposed to Q/m_π and are numerically small. Still, they can be readily computed in EFT. Defining the deuteron mean-square charge radius by $\langle r^2 \rangle_d \equiv 6(dF_C/dq^2)$, one finds

$$\langle r^2 \rangle_d = \langle r^2 \rangle_N + \frac{1}{1 - \gamma\rho} \frac{1}{8\gamma^2} + \frac{1}{32M^2} = 4.565 \text{ fm}^2, \quad 18.$$

to be compared with the experimental value $\langle r^2 \rangle_d = 4.538$ fm^2.

The magnetic form factor $F_M(q^2)$ at LO and NLO is simply the electric form factor $F_C(q^2)$ multiplied by the isoscalar nucleon magnetic moment $\kappa_n + \kappa_p$, except for a new two-body term that appears at NLO without an ERT analog,

$$\mathcal{L} = -eL_2 i\epsilon^{ijk} (NP_i N)^\dagger (NP_j N) B_k + \text{h.c.} \quad 19.$$

The coefficient L_2 can be determined through the experimental value of the deuteron magnetic moment and, using this value, one can predict the momentum dependence of $F_M(q^2)$.

The $F_Q(q^2)$ form factor involves a transition between the S- and D-wave components of the deuteron. At LO, its value is determined by an S- to D-wave transition operator whose coefficient is extracted from the asymptotic D/S ratio of the deuteron, $\eta_{D/S}$. At NLO, there is a new two-body term

$$\mathcal{L} = -eC_Q (NP_i N)^\dagger (NP_j N) \left(\nabla^i \nabla^j - \frac{1}{3} \nabla \delta^{ij} \right) A^0, \quad 20.$$

whose coefficient C_Q can be fitted to the experimental deuteron quadrupole moment. At N^{2}LO, the only contribution comes from the finite size of the nucleon charge distribution $\langle r^2 \rangle_N$. The value of $F_Q(0)$ is then a fit, but the momentum dependence is an EFT prediction. The presence of a counterterm not determined

by *NN* scattering at NLO indicates that μ_Q is sensitive at the ∼10% level to short-distance physics not determined by *NN* scattering. That is probably the reason different potential-model calculations underpredict μ_Q by ≃5%.

Other electromagnetic processes can be studied in similar fashion; the next section shows another example. Compton scattering and deuteron polarizabilities are discussed in References (28, 29).

2.1.3. RADIATIVE CAPTURE OF NEUTRONS BY PROTONS The $n + p \to d + \gamma$ reaction at low energies is a key ingredient in Big Bang nucleosynthesis calculations. The amplitude for this process can be expanded in multipoles as

$$\begin{aligned}\mathcal{A} = {} & ieX_{M1V}\epsilon^{ijk}\epsilon^{*i}k^j\varepsilon^k nP^3 p + eX_{E1V}n\tau_2\tau_3\sigma_2\vec{\sigma}\cdot\vec{\epsilon}^{\,*}pP^i\varepsilon^{*i} \\ & + \frac{eX_{M1S}}{\sqrt{2}}nP^i[k^i\vec{\epsilon}^{\,*}\cdot\vec{\varepsilon}^{\,*} - \vec{\epsilon}^{\,*}\cdot\vec{k}\varepsilon^{*i}]p \\ & + \frac{eX_{E2S}}{\sqrt{2}}\,nP^i\left[k^i\vec{\epsilon}^{\,*}\cdot\vec{\varepsilon}^{\,*} + \vec{\epsilon}^{\,*}\cdot\vec{k}\varepsilon^{*i} - \tfrac{2}{3}\epsilon^{*i}\vec{k}\cdot\vec{\varepsilon}^{\,*}\right]p + \ldots, \end{aligned} \qquad 21.$$

where n and p are the neutron and proton Pauli spinors, k is the photon momentum, and ϵ (ε) is the polarization of the deuteron (photon). At low energies, the form factor X_{M1V} dominates the cross section by a few orders of magnitude. Its computation at LO is the same as the ERT one and underpredicts the experimental value for thermal neutron capture by 10%. This discrepancy was long ago attributed to a pion-exchange current contribution (30). In EFT (15), the same effect is encapsulated in the *NN* current

$$\mathcal{L} = eL_{M1V}(NP^iN)^\dagger(NP^AN)\delta_{A3}B^i + \text{h.c.}, \qquad 22.$$

whose coefficient L_{M1V} can be determined by the cold-capture cross section. The momentum dependence is then predicted. However, for photon energies larger than a few MeV, the X_{E1V} form factor dominates the cross section. Up to N^{3}LO, the computation of X_{E1V} involves only C_{0t}, C_{2t}, the P-wave interaction combination D_P encountered in the polarizability calculation, and L_{M1V} fitted at threshold. At N^{4}LO, some relativistic effects and a new term appear (31):

$$\mathcal{L} = eL_{E1V}(NP^i\mathrm{N})^\dagger[N(\overleftarrow{\nabla}_i\tilde{P}_{jA} - \overleftarrow{\nabla}_j\tilde{P}_{iA})N]\delta_{A3}E^j, \qquad 23.$$

where $\tilde{P}_{iA} = \sigma_2\sigma_i\tau_2\tau_A/\sqrt{8}$, which is fitted using data for the inverse reaction $d+\gamma \to n+p$. Figure 3 shows the resulting cross section for the photodissociation of the deuteron and compares it to data (32). The estimated error is $O(Q/m_\pi)^5 \sim$ 1%. These precise, analytical computations are particularly useful for Big Bang nucleosynthesis codes.

Chen et al. analyzed a set of polarization observables in the $n + p \to \gamma + d$ reaction (33).

2.1.4. NEUTRINO-DEUTERON SCATTERING AND PROTON-PROTON FUSION A complete set of reactions involving (anti-) neutrino breakup of the deuteron was computed in the pionless EFT approach (34). Kong & Ravndal analyzed fusion and the

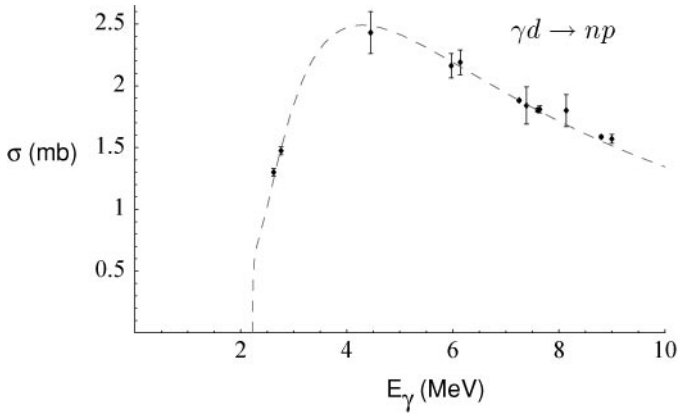

Figure 3 Cross section for $\gamma + d \to n + p$ as a function of the photon energy at N^{4}LO, compared to data. (From Reference (31), courtesy of G. Rupak.)

interplay of Coulomb interactions (35). These reactions are essential for the understanding of solar neutrino physics, since they are relevant for both production ($p + p \to d + e^+ + \nu_e$) and detection in heavy-water detectors (through the neutral-current $\nu + d \to \nu + n + p$ and the charged-current $\overline{\nu} + d \to e^+ + n + n$ reactions).

The weak interactions are described by the familiar neutral and charged-current pieces

$$\mathcal{L} = -\frac{G_F}{\sqrt{2}}\left(l_{Z\mu} J_Z^\mu + l_{+\mu} J_-^\mu + \text{h.c.}\right), \qquad 24.$$

with the leptonic currents $l_{Z\mu} = \overline{\nu}(1-\gamma_5)\gamma_\mu \nu$, $l_{+\mu} = \overline{\nu}(1-\gamma_5)\gamma_\mu e$ and hadronic currents $J_-^\mu = V_-^\mu - A_-^\mu$ and $J_Z^\mu = -2\sin^2\theta_W V_0^\mu + (1-2\sin^2\theta_W)V_3^\mu - A_0^\mu - A_3^\mu$. The isosinglet vector (axial) current V_0^μ (A_0^μ) and isotriplet vector (axial) current V_A^μ (A_A^μ), written in terms of the nucleon fields, have contributions in the form of one- and two-nucleon operators. The one-nucleon operators are determined by the axial coupling constant $g_A = 1.26$, the neutron and proton magnetic moments κ_n and κ_p, the strange contribution to the proton spin $\langle \overline{s}\gamma^\mu\gamma_5 s\rangle$, and the strange magnetic moment of the proton μ_s. The two-nucleon currents contributing up to N^{2}LO are

$$\begin{aligned}
\mathcal{A}_a^i &= L_{1A}(NP^iN)^\dagger(NP_AN),\\
\mathcal{A}_0^i &= -2i\,L_{2A}\epsilon_{ijk}(NP^iN)^\dagger(NP^jN) + \text{h.c.},\\
\mathcal{V}_a^i &= 2i\,L_1\epsilon_{ijk}(NP^jN)^\dagger(\vec{\nabla}^k + \overleftarrow{\nabla}^k)(NP_aN),\\
\mathcal{V}_0^i &= 2i\,L_2(NP^jN)^\dagger(\vec{\nabla}_j + \overleftarrow{\nabla}_j)(NP^iN). \qquad 25.
\end{aligned}$$

$L_1 = L_{M1V}$ was determined through the neutron-proton cold-capture cross section, and L_2 was determined by the value of the deuteron magnetic moment. The parameters L_{2A}, $\langle \bar{s}\gamma^\mu\gamma_5 s\rangle$, and μ_s, which are not well determined experimentally, have a negligible impact on the cross section (<1%) due to the near orthogonality between initial and final states in the triplet channel. The only relevant unknown in a N^{2}LO calculation is then the value of L_{1A}. Using the estimate in Equation 15, we find $L_{1A} \sim 4\pi/M\mu^2 \sim 5$ fm^3. Two potential-model results, one with and another without exchange-current terms, differing by about 5%, can be reproduced by varying the value of L_{1A} within this range. This shows that the difference between these calculations comes from different assumptions about the short-distance physics. To fix this indeterminacy and, consequently, obtain predictions for the νd reactions at the percent level, one must determine the value of L_{1A} experimentally. One possibility is to measure one of these reactions at one energy. The other is to extract L_{1A} through another process sensitive to this term, such as tritium β-decay or muon capture on the deuteron. The challenges involved in this extraction from the well-measured value of the tritium lifetime are discussed below.

2.2. The Three-Body System and the Limit Cycle

Compared with the study of the *NN* sector, the study of 3*N* systems using EFT is still in its infancy. Only now are calculations appearing for the triton-^{3}He channel that are accurate enough to enable precision calculations of processes involving external currents. Those processes may turn out to be a very important way of fixing the value of two-body LECs, which are hard to measure in the deuteron. The new ingredients in going from two- to three-body systems are three-body interactions. In the absence of fine-tuning, their typical size is determined by dimensional analysis. Since they subsume physics contained within the range $1/\Lambda \sim 1/m_\pi$, a three-body force with $2n$ derivatives would have the typical size

$$\mathcal{L}_3 \sim D_{2n}\vec{\partial}^{2n}(N^\dagger N)^3 \to D_{2n} \sim \frac{(4\pi)^2}{M\Lambda^{4+2n}}. \qquad 26.$$

As in the two-body force, the fine-tuning in the two-body *S*-wave channels introduces a new scale $\gamma \sim 1/a_s$ that invalidates the estimate in Equation 26. We resort to the same argument used above to estimate the size of these contributions. We demand that observables be cutoff-independent order by order in the low-energy expansion, which determines the running of the three-body forces if we assume that their typical size is set by the size of their running, $D_{2n}(\Lambda) \sim D_{2n}(2\Lambda) - D_{2n}(\Lambda)$. As mentioned above, it is unlikely that $D_{2n}(\Lambda)$ is much smaller than this estimate for a particular value of the regulator Λ, or that it contains a large Λ-independent piece. If the inclusion of a particular LEC is necessary in order to have cutoff-independent results (at a particular order in the expansion), this LEC needs to be large enough to appear at that same order of the expansion.

The behavior of the doublet *S*-wave channel (where the triton and ^{3}He are) is very different from that of the other channels. The physical reason is that

this is the only channel where all three nucleons can occupy the same point in space (two spin and two isospin states allow for a maximum of four nucleons in the same state). A system of three bosons also displays this property and is qualitatively similar to three nucleons in the doublet *S*-wave channel. In the remaining channels, either the angular-momentum barrier or the Pauli exclusion principle forbids the three nucleons to touch. One would then expect that the doublet *S*-wave channel (and systems of three bosons) are much more sensitive to short-distance physics than the other channels, an expectation that is confirmed by further analysis.

To avoid unnecessary complications, we present explicit expressions only for the case of the *S*-wave three-boson system. The formulae for the nucleon cases in the different channels can be deduced in an analogous way (see e.g., References 36–38). A convenient first step is to rewrite the action in terms of an auxiliary "dimeron" field d (39),

$$\begin{aligned}\mathcal{L}_{\text{bosons}} &= N^\dagger\Big(i\partial_0 + \frac{\vec{\nabla}^2}{2M} + \ldots\Big)N - C_0(NN)^\dagger NN - D_0(NNN)^\dagger NNN + \ldots \\ &\to N^\dagger\Big(i\partial_0 + \frac{\vec{\nabla}^2}{2M} + \ldots\Big)N + \Delta d^\dagger d \\ &\quad + y(d^\dagger NN + dN^\dagger N^\dagger) + g d^\dagger d N^\dagger N + \ldots, \end{aligned} \qquad 27.$$

where $C_0 = y^2/\Delta$ and $D_0 = -gy^2/\Delta^2$. The equivalence between the two Lagrangians above can be shown by simply performing the Gaussian integral over the auxiliary field d. Because d has the quantum numbers of a two-particle bound state, it can be used as an interpolating field for the bound state. The normalization of the field d (and the value of Δ) is arbitrary and all the observables should be a function only of the combinations y^2/Δ and gy^2/Δ^2, not of y, g, and Δ separately.

The propagator $\mathbf{\Delta}(p)$ for the dimeron field of momentum p is given by the sum of bubble graphs at the top of Figure 4. The power counting that leads to

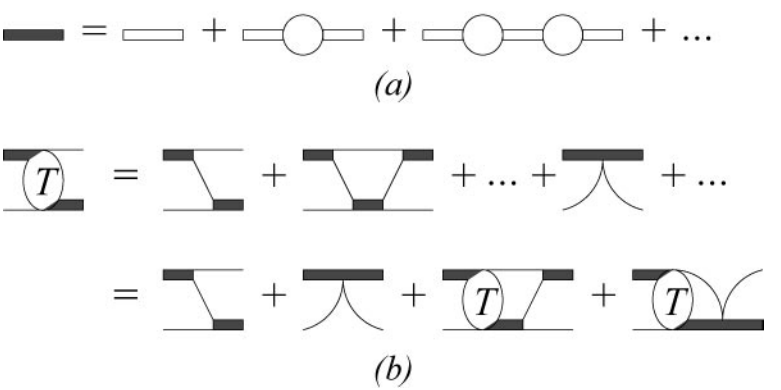

Figure 4 LO graphs contributing to (*a*) the dressed propagator of the dimeron and (*b*) the particle/dimeron amplitude.

the necessity of summing all these graphs when the scattering length is large is identical to the one discussed in connection with *NN* scattering. Taking the arbitrary constant Δ to scale as $\Delta \sim 1$, we have $y^2 \sim C_0 \sim 4\pi/MQ$, and thus $\mathbf{\Delta}(p)$ scales as $\mathbf{\Delta}(p) \sim (4\pi/My^2)(1/Q) \sim 1$. Summing all graphs, we can write

$$\mathbf{\Delta}(p) = \frac{1}{-\gamma + \sqrt{\frac{3p^2}{4} - ME}}. \qquad 28.$$

Let us now consider the graphs that describe the scattering of one particle off the bound state of two others, shown at the bottom of Figure 4. We can determine the impact of each graph by power counting. For each additional loop, we have two particle propagators, one d propagator, two powers of y, and one loop integration, for a total of $(M/Q^2)^2(1)(4\pi/MQ)(Q^5/4\pi M) \sim 1$. There is no suppression for additional loops, and all diagrams that involve an arbitrary number of particle exchanges contribute at LO. Graphs that include the two-body C_2 operator are suppressed and start appearing at NLO. Graphs that include the three-body force may or may not be leading, depending on the size of the three-body forces. Because at this point we do not know how large they typically are, we provisionally include them. The chain of diagrams to be summed, in contrast to the two-particle case, does not form a simple geometrical series and cannot be summed analytically.

We can, however, consider the second line in Figure 4 as an equation that determines this sum. For the bosonic case, $\lambda = 1$, we have

$$t_k(p) = K(p,k) + \frac{2H}{\Lambda^2} + \frac{2\lambda}{\pi}\int_0^\Lambda dq q^2 \mathbf{\Delta}(q)\left(K(p,q) + \frac{2H}{\Lambda^2}\right) t_k(q), \qquad 29.$$

with

$$K(p,q) = \frac{1}{pq}\ln\left(\frac{p^2+pq+q^2-ME}{p^2-pq+q^2-ME}\right),$$

$$H(\Lambda) = \frac{g\Lambda^2}{4My^2}, \qquad 30.$$

where $t_k(p)$ is the scattering amplitude with all but the outgoing single-particle line on-shell ("half-off-shell amplitude"), k is the incoming momentum in the center-of-mass system, p is the outgoing momentum, and $ME = 3k^2/4 - \gamma^2$ is the total energy. The on-shell point is at $p = k$.

In the case of nucleons in the quartet channel, the same equation is obtained, but with $\lambda = -1/2$ and some additional momentum dependence in the three-body force (since the simple momentum-independent three-body force does not contribute to this channel). Because all spins are parallel in the quartet channel, only triplet two-body interactions occur and the value of γ is determined by the deuteron pole. The auxiliary field d carries the quantum numbers of the deuteron. In the doublet case, singlet and triplet two-body interactions contribute. The analog

of Equation 29 is a pair of coupled integral equations that, in the $SU(4)$ limit,[6] where the singlet and triplet scattering lengths are equal (or in the ultraviolet, where $1/a_s$, γ can be discarded), decouple into a pair of equations like Equation 29, one with $\lambda = 1$, another with $\lambda = -1/2$. Two auxiliary fields appear, one with the quantum numbers of the deuteron, another with the ${}^1S_0$ quantum numbers.

In all spin channels, equations for the higher partial waves are obtained by substituting the logarithm in the kernel by a Legendre function $Q_l[pq/(p^2+q^2-ME)]$. Equation 29 is the version of the Faddeev equation (see Reference (41) for an introduction) that is appropriate for contact interactions. It was first derived, by very different methods, in Reference (42). It is only for separable potentials, like the contact interactions considered here, that the Faddeev equation reduces to a one-dimensional integral equation. This simplification reduces the numerical work involved by many orders of magnitude.

2.2.1. MOST CHANNELS ARE EASY Let us first consider the channels in the second group, that is, all channels but the doublet S wave. The diagrams summed by Equation 29 are all ultraviolet finite, which suggests that there is no need to include three-body forces to absorb the cutoff dependence, since this dependence is a subleading $1/\Lambda$ effect. The (numerical) solution confirms this. Even in the absence of a three-body force, the phase shifts are only weakly dependent on Λ, and $t_k(k)$ has a finite limit when $\Lambda \to \infty$. Higher-order corrections can be included either perturbatively (as was done in the two-body sector) or nonperturbatively through the denominator in the dimeron propagator. This last resummation amounts to including some (but not all!) higher-order effects. It can be automatically computed by solving a modified version of Equation 29, which is easier than performing perturbative calculations at high orders. Calculations of the neutron-deuteron phase shifts are presently available up to $\mathrm{N^2LO}$ (12, 36, 37). At this order, the only inputs are γ and r_{0t} (for the three-body quartet channels) and $1/a_s$ and r_{0s} (needed only for the doublet channels). No unknown LECs appear at $\mathrm{N^3LO}$, so this approach can be easily pushed to higher orders (and precision). For a flavor of the results, Figure 5 shows the predicted quartet S-wave phase shift and compares it to a phase-shift analysis (43) (at finite k) and a scattering length measurement (44) (essentially at $k=0$).

Most of the data are not precise enough to provide a strict test of the convergence of the low-energy expansion, but the zero-energy point is much better measured. The EFT calculation gives for the quartet S-wave scattering length $a_{3/2} = 5.09 + 0.89 + 0.35 + \ldots = 6.33 \pm 0.05$ fm (12, 42, 45), whereas the experimental value is $a_{3/2}^{\mathrm{exp}} = 6.35 \pm 0.02$ fm (44). The EFT error is probably overestimated, since the $\mathrm{N^2LO}$ calculation resummed some of the $\mathrm{N^3LO}$ pieces and the remaining ones are known to be smaller than the naive estimate (such as the effect of the two-body shape parameter). Because the whole input in these calculations consisted of the threshold parameters of *NN* scattering, these results are universal and constitute a

[6]See Reference (40) for a discussion of the $SU(4)$ limit in the *NN* sector.

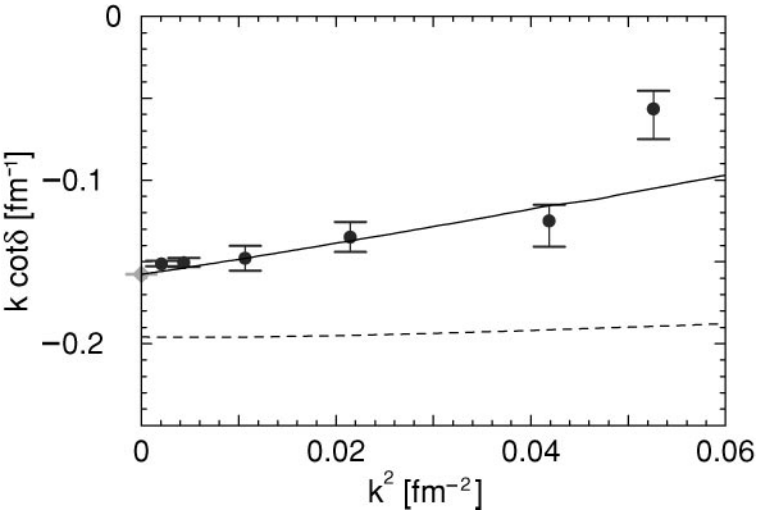

Figure 5 $k \cot \delta$ for neutron-deuteron scattering in the quartet *S*-wave channel as a function of the energy. The dashed line is the LO and the solid line the N^2LO result (36). Points are from a phase-shift analysis (43) and a near-threshold measurement (44). (Figure courtesy of H.-W. Hammer.)

"low-energy theorem." Any model with the correct scattering lengths and effective ranges (barring wildly wrong phase shifts above threshold) should reproduce them, within the estimated error. The small discrepancy with "first-generation" *NN* potentials can be explained by the imprecise values of $a_{s,t}$ that those models predicted. "Second-generation" (or "realistic") potentials fixed this discrepancy (46).

Coulomb interactions are important in proton-deuteron scattering at small energies. Reference (47) shows that they can be easily incorporated in the quartet channels by a simple change in the kernel of Equation 30.

2.2.2. TRITON-^{3}HE CHANNEL AND THE LIMIT CYCLE The opposite sign of λ in the bosonic and quartet equations implies qualitatively different behavior of the respective solutions. The most striking feature is that the solution of the bosonic (and of the *S*-wave doublet) equation in the absence of a three-body force depends sensitively on the value of cutoff used, even though, as mentioned above, there is no ultraviolet divergence in the graphs summed. To illustrate this, Figure 6 shows the $k = 0$ solutions of Equation 29 that correspond to various cutoffs (with $\lambda = 1$, $H = 0$). Notice that the three-body scattering length, determined by the asymptotic plateau on the left, $t_{k=0}(k = 0)$, can take any value as one varies the cutoff within a reasonable range.

It has been known for a long time that Equation 29 is not well-defined in the limit $\Lambda \to \infty$. This disease can be shown in a variety of ways (21, 48–50). Consider

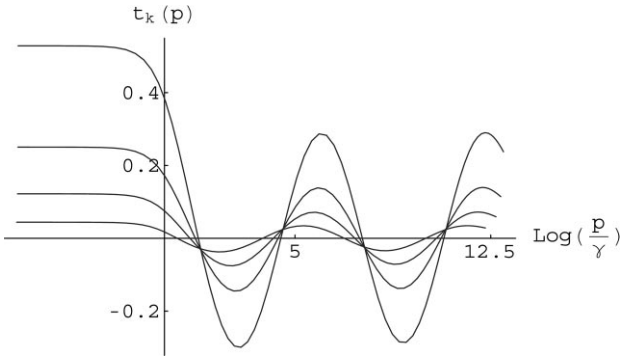

Figure 6 Zero-energy half-off-shell amplitude for boson/two-boson scattering as a function of the outgoing momentum p, from a numerical solution of Equation 29 with no three-body force, for several different cutoffs.

the intermediate-momentum regime $Q \ll p \ll \Lambda$ (remember that Q stands for any infrared scale $Q \sim \gamma \sim k$). Up to terms suppressed by powers of Q/Λ, with the assumption that $H \sim 1$, Equation 29 reduces to (48)

$$t_k(p) = \frac{4}{\sqrt{3}\pi} \int_0^\infty dq \frac{1}{q} \ln\left(\frac{p^2 + pq + q^2}{p^2 - pq + q^2}\right) t_k(q). \qquad 31.$$

Equation 31 has two symmetries,[7]

$$\begin{aligned} &t_k(p) \to t_k(\alpha p) \quad \text{(scale invariance)} \\ &t_k(p) \to t_k(1/p) \quad \text{(inversion symmetry)}, \end{aligned} \qquad 32.$$

which suggest the power-law solution $t_k(p) \sim p^s$. The allowed values of s are determined by plugging this ansatz back into Equation 31. For values of s such that $\mathrm{Re}(s) < 0$, we find

$$\frac{8\lambda}{\sqrt{3}s} \frac{\sin\frac{\pi s}{6}}{\cos\frac{\pi s}{2}} = 1. \qquad 33.$$

For values of λ smaller than $\lambda_c \equiv 3\sqrt{3}/4\pi = 0.4135\ldots$, the roots of Equation 33 have $\mathrm{Re}(s) < -1$ and the half-off-shell amplitude goes rapidly to zero as $p \to \infty$. In the quartet channel, for instance, $t_k(p) \sim 1/p^{3.17}$, which is a softer ultraviolet behavior than the one expected in perturbation theory, $t_k(p) \sim 1/p^2$. For the S-wave doublet case (or the bosonic case), though, $\lambda = 1$ and there is a pair of

[7]These symmetries suggest that in the limit $\gamma, 1/a_s \to 0$ the full conformal symmetry holds. In the two-body sector this was confirmed, even for off-shell amplitudes (51). It is not known whether the three-body amplitude is conformal in this limit. The three-body forces break scale invariance at the order they first appear.

imaginary solutions $s = \pm i s_0$, with $s_0 = 1.006\ldots$. The asymptotic behavior of the half-off-shell amplitude is then

$$t_k(Q \ll p \ll \Lambda) = A \sin(s_0 \ln p + \delta), \tag{34.}$$

where A and δ are p-independent numbers. This oscillatory behavior can be seen in Figure 6.

The normalization A is fixed by the inhomogeneous term in Equation 29. Because that is important only in the infrared region $p \sim Q$, A can be determined only by matching Equation 34 to the solution in the infrared region. The phase δ is determined by matching Equation 34 to the solution in the ultraviolet region and will depend on the ultraviolet physics [such as the value of the regulator Λ and the three-body force $H(\Lambda)$]. Actually, by dimensional analysis, the Λ-dependence of δ has to be of the form $\delta(\Lambda) = -s_0 \ln \Lambda + \bar{\delta}$. If we vary Λ while keeping H constant, as we have done so far, the dependence on the asymptotic phase δ will "spill over" the infrared region and change the on-shell amplitude by a factor of $O(1)$. On the other hand, δ does not depend on the infrared scales (k, γ, $1/a_s$), and so $H(\Lambda)$ can be adjusted so that $\delta = -s_0 \ln \Lambda + \bar{\delta}(H(\Lambda)) \equiv -s_0 \ln \bar{\Lambda}$ is cutoff-independent (for any value of k), with $\bar{\Lambda}$ being a constant. Thus, the requirement of cutoff invariance means that $H(\Lambda)$ runs at LO and, for generic values of Λ, $H(\Lambda) \sim 1$. The typical size of the three-body force is then

$$D_0 \sim \frac{(4\pi)^2 H}{M\Lambda^2 Q^2} \sim \frac{(4\pi)^2}{M\Lambda^2 Q^2}, \tag{35.}$$

as opposed to the naive estimate in Equation 26. This means that D_0 is enhanced in the presence of fine-tuning in the two-body sector by a factor of $(\Lambda/\gamma)^2$. The arbitrary parameter $\bar{\Lambda}$ has to be fixed by one piece of experimental input coming from a three-body observable.

The two-body phase shifts are not sufficient to fix the three-body physics at LO. Another way of looking at the renormalization of the three-body system that is more easily generalizable to higher-order calculations is to consider two amplitudes, $t_k^{\Lambda}(p)$ and $t_k^{\Lambda'}(p)$, which are obtained by solving Equation 29 with two cutoffs Λ and Λ' and the corresponding three-body forces $H(\Lambda)$ and $H(\Lambda')$. The integral equation that determines $t_k^{\Lambda'}(p)$ can be written as

$$\begin{aligned}
&\int_0^{\Lambda} dq \left(\delta(p-q) - \frac{2}{\pi} q^2 \mathbf{\Delta}(q) K(p,q)\right) t_k^{\Lambda'}(q) \\
&\quad = K(p,k) + \frac{2H(\Lambda)}{\Lambda^2} + \frac{2}{\pi}\frac{2H(\Lambda)}{\Lambda^2}\int_0^{\Lambda} dq q^2 \mathbf{\Delta}(q) t_k^{\Lambda'}(q) \\
&\qquad + \frac{2H(\Lambda')}{\Lambda'^2} - \frac{2H(\Lambda)}{\Lambda^2} + \frac{2}{\pi}\left(\frac{2H(\Lambda')}{\Lambda'^2} - \frac{2H(\Lambda)}{\Lambda^2}\right)\int_0^{\Lambda} dq q^2 \mathbf{\Delta}(q) t_k^{\Lambda'}(q) \\
&\qquad + \frac{2}{\pi}\int_{\Lambda}^{\Lambda'} dq q^2 \mathbf{\Delta}(q)\left(K(p,q) + \frac{2H(\Lambda)}{\Lambda^2}\right) t_k^{\Lambda'}(q).
\end{aligned} \tag{36.}$$

The first two lines in Equation 36 are identical to the equation that determines $t_k^\Lambda(p)$. If the effect of the remaining terms is small [up to terms of $O(Q/\Lambda)$], $t_k^\Lambda(p) = t_k^{\Lambda'}(p)$ [again, up to terms of $O(Q/\Lambda)$]. These terms are indeed small, suppressed by a factor of Q/Λ compared with the leading terms. However, their effect on $t_k^\Lambda(p)$ is not suppressed. That is because the operator acting on $t_k^\Lambda(p)$ on the left-hand side of Equation 36 is nearly singular, that is, it has a small eigenvalue of $O(Q/\Lambda)$, so that

$$\int_0^\Lambda \left(\delta(p-q) - \frac{2}{\pi} q^2 \mathbf{\Delta}(q) K(p,q)\right) a(q) = O(Q/\Lambda) a(p). \qquad 37.$$

The eigenfunction $a(p)$ has the same asymptotics shown in Equation 34 as $t_k^\Lambda(p)$. In our determination of the asymptotics, Equation 34, we have already shown Equation 37 in the limit $\Lambda \to \infty$ and the total energy $E \to 0$. We now see that the operator on the left-hand side of Equation 36 is almost noninvertible and that the projection of $t_k^\Lambda(p)$ in the $a(p)$ direction is sensitive to the $O(Q/\Lambda)$ terms on the right-hand side of Equation 36. The amplitudes computed with different Λs, shown in Figure 6, indeed differ in the intermediate regime by a term of the form $\sin(s_0 \ln p + \delta)$. The solution $t_k^\Lambda(p)$ has an increased sensitivity to the ultraviolet physics and changes by a factor of $O(1)$ if the right-hand side of Equation 36 changes by a factor of $O(Q/\Lambda)$. That explains the apparent contradiction between the cutoff sensitivity and the absence of ultraviolet divergences.

If we use the asymptotic form of $t_k^\Lambda(p)$, Equation 34, even in the region $p \sim \Lambda$ where it is unjustified, and drop the terms suppressed by $(Q/\Lambda)^2$, we can derive an approximate analytical expression for $H(\Lambda)$ needed to cancel the Q/Λ terms in Equation 36 [and to guarantee $t_k^\Lambda(p)$ is cutoff-independent up to $O(Q/\Lambda)$]:

$$H(\Lambda) = \frac{\cos\left(s_0 \ln(\Lambda/\overline{\Lambda}) + \arctan s_0\right)}{\cos\left(s_0 \ln(\Lambda/\overline{\Lambda}) - \arctan s_0\right)}, \qquad 38.$$

where $\overline{\Lambda}$ is the parameter that determines the asymptotic phase, to be fixed by experiment. We show $H(\Lambda)$ in Figure 7. The points there were determined by numerically finding values of $H(\Lambda)$ that, when inserted in Equation 29, reproduce the same three-body phase shifts for different values of Λ. The solid line is Equation 38. The agreement between Equation 38 and the numerical points, as well as the independence of the phase shifts with Λ after $H(\Lambda)$ is properly changed, confirms our understanding of this somewhat unusual renormalization. For further discussion of renormalization-group invariance at this order, see Reference (52).

The asymptotic running of the three-body coupling can be interpreted as a limit cycle. The possibility of limit cycles in addition to fixed points was suggested in Reference (53) but apparently never before seen in a simple physical system. Limit cycles are now being further studied (54).

NLO calculations of phase shifts were performed in Reference (55) (scattering lengths were computed by different but equivalent methods in References 49 and 45). No new three-body force is needed at this order, although $H(\Lambda)$ has

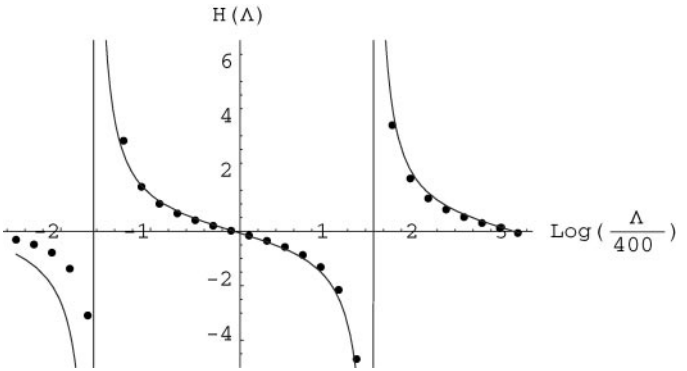

Figure 7 Three-body force coefficient $H(\Lambda)$ computed analytically (line) and numerically (points) as a function of $\log(\Lambda/400\ \text{MeV})$.

a correction proportional to the two-body effective range. As in other channels, it is convenient to compute higher-order corrections by computing the kernel at the order desired and iterating it. That is, one numerically solves Equation 29 with a kernel that includes higher-order effects. At NLO, we demand $t_k^{\Lambda}(p)$ to be independent of Λ up to terms of $O(Q/\Lambda)^2$. Due to the almost singular nature of the integral equation, the right-hand side of Equation 36 must be Λ independent up to terms of $O(Q/\Lambda)^3$. This can be accomplished with the same no-derivative three-body force because the terms of $O(Q/\Lambda)^2$ on the right-hand side of Equation 36 are k- and p-independent. [However, $H(\Lambda)$ will have a different form than in Equation 38]. Similarly, at N^{2}LO we need to cancel the $O(Q/\Lambda)^3$ terms on the right-hand side. Those terms, however, are proportional to k^2 and p^2 and can be absorbed only by a three-body force with two derivatives. So, at N^{2}LO, a new three-body force appears, and we need yet another piece of three-body data to fix this new LEC.

The cutoff sensitivity is dramatically reduced by going to higher orders, as expected (56). Figure 8 shows the phase shifts in the S-wave doublet channel computed at the first three orders (56). As inputs in these calculations, besides the two-body interactions, we have a no-derivative three-body force fitted to the experimental binding energy of the triton at LO and a two-derivative three-body force fitted to the experimental value of the doublet neutron-deuteron scattering length at N^{2}LO. The EFT results are compared to a phase-shift analysis (43) and to results from the Argonne V18 potential plus the Urbana three-body force adjusted to reproduce the correct triton binding energy ((57); A. Kievsky, private communication).

The existence, even at LO, of a parameter not determined by *NN* scattering means that models tuned to reproduce the low-energy *NN* phase shifts may differ widely in their predictions for three-body properties. However, since up to NLO

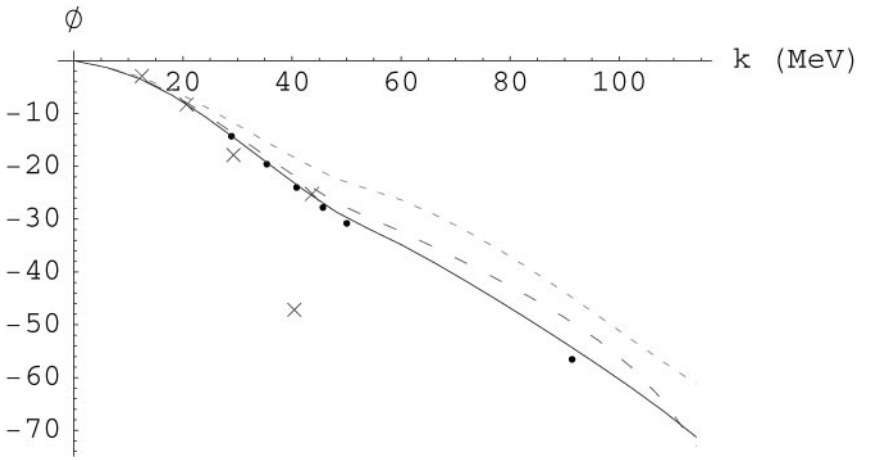

Figure 8 Neutron-deuteron phase shift (in degrees) in the doublet *S*-wave channel as a function of the center-of-mass momentum: EFT at LO (dotted line), at NLO (dashed line), and at N^2LO (solid line); a phase-shift analysis (crosses); and a potential model (points). (From Reference (56) with permission.)

there is only a one-parameter arbitrariness in the three-body predictions, there must be correlations among these predictions. This has been noted empirically (58). Figure 9 shows results for the doublet *S*-wave scattering length and the triton binding energy from a number of models, all of which reproduce the same low-energy *NN* scattering (59). The predictions cover a wide range but show a clear correlation ("Phillips line"). Also shown are the LO and NLO predictions for this correlation, obtained by varying the value of the three-body force at fixed cutoff. An equivalent explanation for the existence of the Phillips line was first offered in Reference (60). Analogous results can be obtained in the EFT for the hypertriton (61).

In the 3*N* system, the pionless EFT seems to converge over a range of momenta that is large enough to include the interesting physics associated with the bound states. For example, if the three-body force is fitted to the scattering length, the binding energy of triton is $B_3 = 8.08 + 0.23 + \ldots = (8.31 + \ldots)$ MeV (38, 56), to be compared to the experimental result $B_3^{\text{exp}} = 8.48$ MeV. The success of these EFT calculations opens the way for the study of low-energy reactions involving triton and ^{3}He.

3. EFFECTIVE FIELD THEORY WITH EXPLICIT PIONS

As the typical momentum Q approaches the pion mass m_π, it becomes increasingly difficult to account for pion exchange as a short-range effect. As we further increase momenta past $Q \sim m_\pi$, we must include in the EFT an explicit pion field and build up all its interactions allowed by symmetries. Because numerically the mass

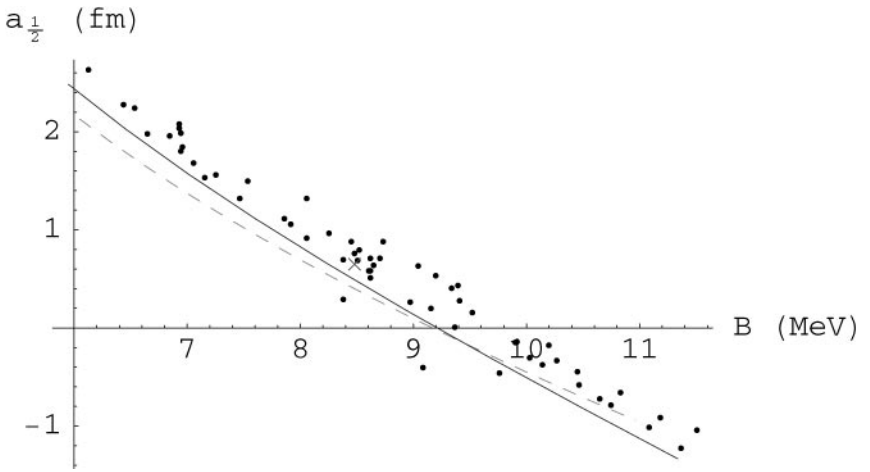

Figure 9 Correlation between the doublet *S*-wave nucleon-deuteron scattering length and the triton binding energy (Phillips line): predictions of different models (points), EFT at LO (light dashed line) and NLO (dark solid line), and experimental value (cross).

difference between the Δ isobar and the nucleon, $\delta m = m_\Delta - m_N$, is $\sim 2m_\pi$, convergence of the pionful EFT is optimized by the concomitant inclusion of an explicit Δ degree of freedom. The Δ can be included without additional problems, since at these momenta the Δ is, like the nucleon, a nonrelativistic object. All other degrees of freedom can be considered heavy. Their effects are still subsumed in contact interactions, as they were in the pionless EFT. What we are doing is removing part of the pion (and possibly the isobar) contributions from the contact interactions. One hopes the new EFT works for momenta up to $M_{\rm QCD} \sim 1$ GeV, the mass scale of the heavier particles.

Adding explicit pions to the theory will generate all sorts of nonanalytic contributions to nuclear amplitudes. We want to devise a rationale for a controlled expansion in the presence of pions.

3.1. Chiral Symmetry and Chiral Perturbation Theory

Fortunately, pion interactions are not arbitrary. Once explicit pion fields are considered, approximate chiral symmetry imposes important restrictions on the way pions couple among themselves and to other degrees of freedom.

In the "chiral limit" where we neglect the masses m_u and m_d of the up and down quarks, QCD has a chiral $SU(2)_L \times SU(2)_R$ symmetry. Because this symmetry is not manifest in the QCD spectrum, it is reasonable to assume that it is broken spontaneously down to its diagonal subgroup, the $SU(2)_{L+R}$ of isospin. Goldstone's theorem (62) tells us that massless Goldstone bosons, naturally identified as pions,

are associated with the three broken generators, and their fields $\boldsymbol{\pi}$ live on the "chiral circle" (actually a three-sphere S^3) that represents the set of possible vacua. We call the radius of this sphere f_π; it is directly related to the chiral-symmetry-breaking scale, $\Lambda_{\chi\mathrm{SB}} \sim 4\pi f_\pi \sim M_{\mathrm{QCD}}$, but the precise factor can only be obtained from the (so far elusive) mechanism of dynamical symmetry breaking in QCD. It turns out that this radius can be determined from the pion lifetime; it is called the pion decay constant, $f_\pi \simeq 92.6$ MeV.

To parameterize the chiral circle, it is convenient to choose fields for which chiral symmetry is respected term-by-term in the effective Lagrangian. Because the interactions of pions have to be invariant under chiral rotations, it is possible to choose fields where an infinitesimal rotation is represented as $\boldsymbol{\pi} \to \boldsymbol{\pi} + \boldsymbol{\epsilon}$. Interactions of these fields always involve derivatives on the sphere, that is, derivatives along with certain nonlinear self-interactions.

As long as quark masses are small enough, they change this picture only slightly. A common quark mass breaks chiral symmetry explicitly down to the diagonal subgroup. Points on the chiral circle are no longer degenerate in energy, and a particular minimum is selected, in a direction given by the quark mass terms that we define as the fourth direction. The quark mass difference further breaks isospin explicitly. In the low-energy EFT, the effect of quark mass terms can be reproduced if we construct all terms that break chiral symmetry in the same way. These interactions can involve $\boldsymbol{\pi}$ without derivatives but are always accompanied by powers of $m_u + m_d$ or $m_u - m_d$. One example is a pion mass term, $m_\pi^2 \propto (m_u + m_d)$. Electromagnetic and weak interactions can be constructed as well.

The well-studied theory of nonlinear representations of symmetries (63) provides the tools to write down the appropriate interactions between pions and other fields. The resulting chiral Lagrangian $\mathcal{L}$ has an infinite number of terms that can be grouped according to the index Δ:

$$\mathcal{L} = \sum_{\Delta=0}^{\infty} \mathcal{L}^{(\Delta)}, \; \Delta \equiv d + f/2 - 2, \qquad 39.$$

where d is the number of derivatives, powers of m_π and/or powers of δm, and f is the number of fermion fields. Because of chiral symmetry, pion interactions that stem from QCD bring derivatives and/or powers of the pion mass. As a consequence, $\Delta \geq 0$. The explicit form of $\mathcal{L}^{(\Delta)}$ for the lower values of Δ can be found in the literature (18, 64).

As in the pionless EFT, the only hope of any predictive power rests on finding some ordering of contributions to amplitudes. This can be done for processes where all the external three-momenta are $Q \sim m_\pi$. Powers of Q of any particular Feynman diagram can be counted as for the superficial degree of divergence. Each space derivative in an interaction produces a three-momentum in a vertex and therefore counts as Q. A complication in the counting of energies stems from the presence of heavy particles such as the nucleon along with light particles such as the pion. In any loop, integration over the zeroth component of the four-momentum will

involve two types of poles, according to the scales appearing in the propagators: (*a*) standard poles at $\sim Q$ that correspond to external three-momenta and to the mass of the pion, and (*b*) shallow poles at $\sim Q^2/2m_N$ that correspond to external nucleon energies.

Processes that involve at most one heavy particle ($A = 0, 1$) are the simplest because the contour of integration can always be closed so as to avoid shallow poles. In this case, all energies are $\sim Q$. As a consequence, each time derivative counts as Q and four-momentum integration brings a factor Q^4. A pion propagator is Q^{-2} and a nucleon (or Δ) propagator is Q^{-1} from its static term; kinetic terms are of relative $O(Q/m_N)$ and thus can be treated as corrections. With these ingredients, one can write the contribution of any diagram to the amplitude as

$$T \propto Q^{\nu}\mathcal{F}(Q/\Lambda), \tag{40.}$$

where Λ is a renormalization scale, $\mathcal{F}$ is a calculable function of LECs, and ν is a counting index. For strong interactions (65),

$$\nu = 4 - 2C - A + 2L + \sum_i \Delta_i, \tag{41.}$$

where $C = 1$ is the number of connected pieces, L is the number of loops, and the sum runs over all vertices. In addition, electroweak interactions can be considered through a simultaneous expansion in $\alpha = e^2/4\pi$ and $G_F f_\pi^2$. Since $L \geq 0$ and $\Delta \geq 0$, $\nu \geq 2 - A \equiv \nu_{\rm min}$. Assuming that all LECs have "natural" size (given by powers of $M_{\rm QCD}$ once the lower scales have been identified explicitly), an expansion in $Q/M_{\rm QCD}$ results. Its first two orders are equivalent to the current algebra of the 1960s, but at higher orders unitarity corrections can be accounted for systematically. In the sector of $A = 0, 1$, the EFT is called chiral perturbation theory (χPT).

In processes that involve more than one stable heavy particle ($A \geq 2$), on the other hand, a failure of perturbation theory can lead to bound states (6). The shallow poles cannot be avoided: they represent "reducible" intermediate states that, as in the pionless EFT, differ from initial states only by nucleon kinetic energies, which are $\sim Q^2/m_N$. This $O(m_N/Q)$ infrared enhancement over intermediate states where energies are $\sim Q$ invalidates Equation 41 for reducible diagrams. Fermion lines, loops, and derivatives then scale with Q as in Equation 16. A pion propagator still counts as Q^{-2}, but the pion can be taken in first approximation as static, and it is sometimes referred to as a "potential" pion. Contributions that come from standard poles naively scale as in processes with no more than one heavy particle. Pions there are nonstatic or "radiative."

The issue now is how to estimate the size of pion contributions. One needs to find the importance of (*a*) pion exchange relative to short-range interactions, and (*b*) multi-pion exchange relative to one-pion exchange (OPE). Both issues are related, via renormalization, to the size of the contact interactions. How large are they in the pionful EFT? What are the contributions that must be resummed in nuclear amplitudes?

3.2. The Two-Nucleon System

As we have discussed, the *NN* system is characterized by scattering lengths a_s and a_t that are much larger than $1/M_{\rm QCD}$. In the pionless theory, this fine-tuning cannot be explained, but it can be accommodated in the power counting by assigning to the contact interactions the scaling given in Equation 16.

A new scale appears naturally in the pionful theory. The leading ($\Delta = 0$) coupling of the pion to the nucleon is derivative with a coupling constant g_A/f_π, where $g_A \simeq 1.26$ is a parameter not fixed by symmetry but determined in β-decay. The OPE contribution to the *NN* amplitude is, schematically, $g_A^2 Q^2/f_\pi^2(Q^2+m_\pi^2)$. Because a reducible intermediate state contributes $m_N Q/4\pi$, relative to OPE, once-iterated OPE can be estimated to give a contribution

$$\frac{\left[g_A^2 Q^2/f_\pi^2\left(Q^2+m_\pi^2\right)\right]^2 (m_N Q/4\pi)}{g_A^2 Q^2/f_\pi^2\left(Q^2+m_\pi^2\right)} \sim \frac{Q}{M_{NN}} \qquad 42.$$

(as long as $Q \gtrsim m_\pi$). Here we introduced the scale

$$M_{NN} \equiv \frac{4\pi f_\pi^2}{g_A^2 m_N}, \qquad 43.$$

which sets the relative strength of multi-pion exchange. Numerically (for $N_c = 3$), $m_N \sim 4\pi f_\pi$ and $g_A \sim 1$, so $M_{NN} \sim f_\pi$. This naive dimensional analysis cannot, however, capture the numerical factors that actually set the relative size of pion contributions. A more accurate estimate requires concrete calculations.

3.2.1. PERTURBATIVE PIONS For $Q \lesssim M_{NN}$, iteration of OPE should be suppressed with respect to OPE according to Equation 42. Moreover, if we assume that the leading short-range effects are $\sim 4\pi a/m_N$ (as in Equation 16 with $Q \to 1/a$), then OPE is suppressed by $O(1/aM_{NN})$ compared with the leading contact interaction. With such estimates, if M_{NN} is sufficiently large (compared with $1/a$ and m_π) and Q sufficiently small, pions may be treated perturbatively. Lutz ((66); private communication) and Kaplan, Savage & Wise (23) suggested that this could be profitable.

A simple power counting, known as KSW counting, follows from taking $Q \sim 1/a \sim m_\pi < M_{NN}$ and counting powers of the light scale Q. This is a direct extension of the power counting in Equation 16. In particular, the scaling of the contact operators is assumed to be the same as before with $\Lambda \to M_{NN}$, and thus their ordering is unchanged. Because of chiral symmetry, each insertion of a pion exchange brings a factor of Q/M_{NN}. Electroweak interactions can be treated in much the same way as before. One can show that renormalization can be carried out consistently within this power counting (23).

However, for this power counting to be relevant to nuclear physics, M_{NN} has to be sufficiently large. If M_{NN} is not larger than m_π, the domain of perturbative pions is no larger than that of the simpler pionless theory. The issue of the range of validity of the EFT with perturbative pions can only be settled by explicit calculation of

dimensionless factors and comparison with precise observed quantities, this being done to sufficiently high order so that a significant number of pion effects can be tested.

With this power counting, the LO *NN* amplitude coincides with that in the pionless EFT (see Figure 1). At this order, there are contributions only in the two *S*-wave channels from chirally symmetric, nonderivative contact interactions (the C_0 terms). Subleading terms, of relative order (Q/M_{NN}), are constructed in a direct extension of subleading terms of the pionless EFT. Besides two two-derivative contact interactions (C_2 terms), we also insert OPE and two nonderivative contact interactions that break chiral symmetry explicitly ($m_\pi^2 C_2^{qm}$ terms). Both C_2 and C_2^{qm} contact interactions only contribute to *S* waves. The tensor operator from OPE, on the other hand, introduces mixing between ${}^3S_1$ and ${}^3D_1$ waves. To this order, all but the *S*-wave phases are predicted in terms of pion parameters. A calculation of the *NN* system to NLO has been done (23, 67). Comparison with the Nijmegen phase-shift analysis (26) suggests that $M_{NN} \simeq 300$ MeV (23). The relative size of OPE and contact interactions was extensively discussed (68–70), but the issue is clouded by the details of fitting procedures.

At N^{2}LO, we encounter new pion exchanges: both nonstatic (or radiative) OPE and once-iterated OPE. A calculation at this order was carried out in all *S*, *P*, and *D* waves (71, 72). In singlet channels, such as ${}^1S_0$, there seems to be good agreement with the Nijmegen phase-shift analysis, but in triplet channels, such as ${}^3S_1$, ${}^3D_1$, and ${}^3P_{0,2}$, the N^{2}LO corrections are big at momenta $\sim$100 MeV and lead to large disagreement (Figure 10 shows one example). The effects of perturbative pions (and of Δ isobars) are milder in the higher partial waves (73).

The problem can be traced to the iteration of the tensor part of OPE. These results suggest that pions, or, more explicitly, the Yukawa part of potential and radiation pions, when treated perturbatively, give rise to a converging expansion for the ${}^1S_0$ scattering amplitude up to fairly large momenta. However, OPE in the ${}^3S_1 - {}^3D_1$ coupled channels is not perturbatively convergent for momenta around 100 MeV, because the tensor force, which survives in the chiral limit, is too large. This, in turn, suggests that the naive estimate $M_{NN} \sim f_\pi$ is not entirely unreasonable.

3.2.2. RENORMALIZATION OF THE PION LADDER AND POWER COUNTING If indeed $M_{NN} \ll M_{\rm QCD}$, we might hope to improve on the expansion of the previous section by a controlled resummation of terms that go as Q/M_{NN}. If $M_{NN} \sim 100$ MeV, the lack of other known particle thresholds there suggests that the resummation could involve pions exclusively. Indeed, Weinberg, who first attempted the use of EFT in the derivation of nuclear forces (6), had already suggested a power counting in which pions appear in LO, and should therefore be iterated. [Some elements of this power counting had been anticipated by Friar (74).]

Weinberg's original proposal (6) for an EFT describing multinucleon systems was to split the full amplitudes into reducible and irreducible parts. Irreducible diagrams, in which typical energies superficially resemble those in ordinary χPT,

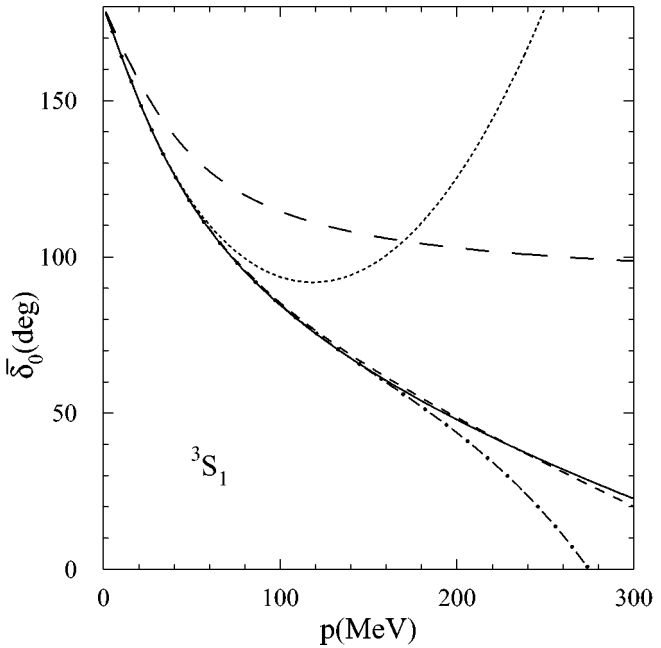

Figure 10 $^3S_1$ *NN* phase shift in the EFT with perturbative pions, as a function of the center-of-mass momentum. The long-dashed, short-dashed, and dotted lines are, respectively, the EFT results at LO, NLO, and N^{2}LO. The dash-dotted line is the N^{2}LO result with a higher-order contact interaction added. The solid line is the Nijmegen phase-shift analysis. (From Reference (72), courtesy of T. Mehen.)

should satisfy the power counting, Equation 41. We call the sum of irreducible diagrams the potential V. Note that the potential, being a set of subgraphs, can be defined in alternative ways. All definitions that exclude the infrared-enhanced contributions but differ by a smaller amount are equally good, provided they avoid double counting and omissions. A field redefinition might change the potential but not the full amplitude. The important point is that the only scale that appears explicitly in the potential is Q, so that the power counting proceeds as in the case of diagrams with at most one heavy particle. Reducible diagrams can be obtained by sewing together irreducible diagrams via intermediate states that contain the propagation of only the initial particles. The full amplitude T for an A-nucleon system is thus a sum of the potential and its iterations; schematically,

$$T = V + VG_0V + VG_0VG_0V + \ldots = V + VG_0T, \qquad 44.$$

where G_0 is the A-nucleon free (Schrödinger) Green's function. This is simply the Lippmann-Schwinger equation, which is formally equivalent to the Schrödinger equation with the potential V, from which wave functions $|\psi\rangle$ can be constructed.

Unfortunately, counting powers of Q is not in itself sufficient for an ordering of interactions. We need to find which other scales accompany Q. Given that we lack a full solution of QCD, we must make some assumptions about the LECs. Because OPE has short-range components, it is natural to assume that they set the scale for the short-range interactions. In this case, since OPE is $O(g_A^2/f_\pi^2)$ for $Q \sim m_\pi$, we expect the leading *NN* contact interactions to be $O(4\pi/m_N M_{NN})$. This hypothesis explains why nuclear bound states are much shallower than naively expected (6, 9). The series in Equation 44 is roughly

$$T \sim \frac{4\pi}{m_N M_{NN}}\left[1 + O\left(\frac{Q}{M_{NN}}\right) + \dots\right], \qquad 45.$$

which requires resummation and exhibits a (real or virtual) bound state at $Q \sim M_{NN}$. In other words, the natural scales for the *NN* scattering length and for the binding energy of a nucleus are

$$|a| \sim \frac{1}{M_{NN}}, B \sim \frac{M_{NN}^2}{m_N} \sim \frac{\left(4\pi f_\pi^2\right)^2}{g_A^4 m_N^3}, \qquad 46.$$

respectively. We find that it is not $M_{\rm QCD}$ by itself that sets the scale for binding energies, but a certain ratio of powers of f_π and m_N. If we estimate $m_N \sim 4\pi f_\pi$ and $g_A \sim 1$, then $B \sim f_\pi/4\pi \sim 10$ MeV. It remains mysterious why the *NN* (real and virtual) bound states are even shallower, or equivalently, why $|a|$ is a few times the natural scale of $1/M_{NN}$. This still has to be accommodated by fine-tuning the contact interactions.

Because LECs serve as counterterms to pion loops in the potential, which are expected to be suppressed (as in χPT) by powers of $Q/4\pi f_\pi$, Weinberg implicitly assumed that LECs related to more derivatives and powers of the pion mass contain inverse powers of $M_{\rm QCD}$. That is, a (renormalized) contact operator with index Δ would scale as

$$C_\Delta \sim \frac{4\pi}{m_N M_{NN} M_{\rm QCD}^\Delta}, \qquad 47.$$

as in naive dimensional analysis.

Accepting this assumption and disregarding the fine-tuning, a simple power counting results from taking $Q \sim M_{NN} \sim 1/a \sim m_\pi$. The potential obeys Equations 40 and 41. The leading potential consists of no-derivative, chirally symmetric contact interactions plus static OPE,

$$V^{(0)} = C_0^{(S)} + C_0^{(T)}\vec{\sigma}_1\cdot\vec{\sigma}_2 - \left(\frac{g_A}{f_\pi}\right)^2 \boldsymbol{t}_1\cdot\boldsymbol{t}_2\frac{\vec{\sigma}_1\cdot\vec{q}\,\vec{\sigma}_2\cdot\vec{q}}{\vec{q}^{\,2}+m_\pi^2}, \qquad 48.$$

where $\vec{\sigma}_i$ ($2\boldsymbol{t}_i$) are the Pauli matrices in spin (isospin) space and $\vec{q}$ is the momentum transferred. All contributions to nuclear forces other than Equation 48 would come as corrections in powers of $Q/M_{\rm QCD}$, starting at $(Q/M_{\rm QCD})^2$. The structure of the potential rapidly becomes more complex with increasing order (7). The leading

potential has to be resummed, whereas corrections can be treated in perturbation theory. If the corrections are truly small, resumming them should cause no major loss of control. This method requires numerical solution of the Schrödinger equation and is similar in spirit to the traditional potential-model approach. As we demonstrate below, Weinberg's power counting has been extensively and successfully developed during the past decade to study processes that involve few-nucleon systems.

However, there is a subtlety not present in χPT. Loops in reducible diagrams probe high energies (when nucleons are far off-shell). As in the pionless EFT, the potential does not vanish at large momenta; it is singular. In addition to the δ function and its derivatives already present in the pionless theory, pion exchange generates potentials that behave as $1/r^n$ with $n \geq 3$, as the radial coordinate $r \to 0$. The large-momentum or short-distance behavior is the same as in the chiral limit $m_\pi^2 \to 0$. Even at LO, the tensor force goes as $1/r^3$ in the chiral limit. As a consequence of ultraviolet divergences generated by the iteration of the potential, the infrared enhancement of $M_{\rm QCD}/M_{NN}$ might contaminate LECs, possibly invalidating Equation 47.

The crucial issue is whether, at any given order, all divergences generated by iteration can be absorbed in the parameters of the potential truncated at that order. There is some indication that equally good fits can be achieved in leading orders with various cutoffs (9, 70, 75–78), as required of a sensible EFT, but the numerical nature of the results makes a definite answer difficult.

Unfortunately, there seem to be formal inconsistencies in Weinberg's counting (23, 69). Divergences that arise in the iteration of LO interactions apparently cannot be absorbed by the LO operators themselves. Two examples are two-loop diagrams where (*a*) OPE happens between two contact interactions, with a divergence proportional to the square of the pion mass (23), or (*b*) OPE is iterated three times, with a divergence proportional to the square of the momentum (69). Although these two particular cases could be resolved by promoting two counterterms to LO, it is likely that a similar problem would show up at higher orders in the expansion. The correspondence between divergences and counterterms appears to be lost, a fundamental problem with both the chiral expansion and the momentum expansion that results from Weinberg power counting.

This argument is not decisive, though. In the context of the Schrödinger equation, perturbative arguments are not in general reliable for singular potentials (79). The perturbative expansion might have a cut starting at $g_A^2/f_\pi^2 = 0$; a g_A^2/f_π^2 expansion would then entail correlated contributions to counterterms at different orders, each bringing powers of $M_{\rm QCD}/M_{NN}$ yet resulting in a much better behaved sum. How can the resummation be consistent? There is a mapping between the singular two-body $1/r^2$ central potential and the three-body problem with short-range interactions. In Section 2.2.2, we saw that for the latter, the renormalization of the nonperturbative equation is very different from the renormalization of individual terms in the associated perturbative series (21). In particular, the relevant counterterm exhibits a limit-cycle behavior.

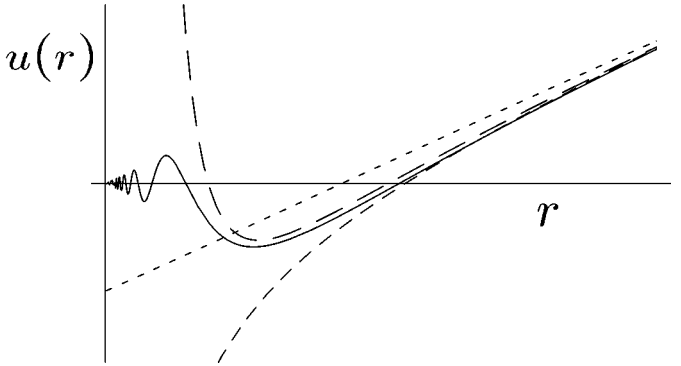

Figure 11 Zero-energy radial wave functions of the $1/r^4$ potential: exact (solid line) and perturbation theory to LO (short dashes), NLO (medium dashes), and N^{2}LO (long dashes). (From Reference (80) with permission.)

It turns out that the correct renormalization of singular potentials is intrinsically nonperturbative (79, 80). Both solutions of the Schrödinger equation for an attractive $1/r^n$ central potential, in contrast to regular potentials, are equally acceptable: the radial wave function $u(r)$, whose large-distance behavior determines low-energy observables, oscillates rapidly as r decreases. Perturbative approximations to the wave function fail at distances comparable to the intrinsic scale r_0 present in the potential, as illustrated in Figure 11. A single counterterm associated with the short-distance physics can render the problem cutoff-independent. For example, short-distance physics can be represented by a square-well potential of radius $R \ll r_0$, whose depth, $V_0 = V_0(R)$, can be adjusted so that physics at $r \gtrsim r_0$ is independent of R (80). [The advantage of this coordinate-space regulator is that one can do an analytic matching of the outer and inner solutions of the Schrödinger equation, thus finding the desired $V_0(R)$. For another technique to deal with a singular potential, see e.g. Reference (81).] Whereas for a repulsive potential there exist only fixed points (82), the situation in the attractive case is similar to the three-body system.

These results were extended to the *NN* potential in the ${}^1S_0$ and ${}^3S_1 - {}^3D_1$ channels (83); the long-range part of the potential was taken as OPE for $r > R$. The asymptotic behavior is that of the chiral limit, where the relevant scale is $r_0 \sim 1/M_{NN}$. The depths of the short-range part of the potential can be different in the singlet and triplet channels, as there are two parameters [$C_0^{(S)}$ and $C_0^{(T)}$] in Equation 48.

In the ${}^1S_0$ channel, the calculation is straightforward. The pion potential is simply a Yukawa form, and the explicit solution is

$$V_0(R;n) = -(2n+1)^2 \frac{\pi^2}{4m_N R^2} - \frac{g_A^2 m_\pi^2}{8\pi f_\pi^2 R} \log\left(\frac{R}{R_*}\right) + O(R^0), \qquad 49.$$

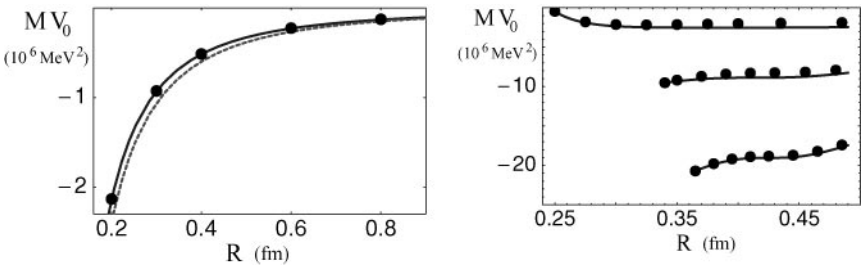

Figure 12 Running of $m_N V_0$ as a function of the cutoff R. Singlet channel (*left panel*): The solid line shows Equation 49 for $n = 1$; the dotted line omits the R^{-1} part. Triplet channel (*right panel*): numerical solution of an analytic matching equation (solid lines). Points are extracted directly from a numerical solution of the Schrödinger equation in the respective channel. (From Reference (83) with permission from Elsevier Science.)

where R_* is an intrinsic length scale to be determined numerically from a fit to low-energy data, and n labels the branch of a cotangent. In the left panel of Figure 12, the R-dependence of V_0, as given by Equation 49, is compared to the numerical solution of the Schrödinger equation with the observed singlet scattering length. The presence of a multibranch structure is related to the accumulation of bound states inside the square well. The presence of unphysical bound states is innocuous if the binding energies of such states are near the cutoff of the EFT.

The formal problem with the chiral expansion in Weinberg's counting survives the resummation. Although the first cutoff-dependent term in Equation 49 can be represented by a chiral-symmetric contact interaction, the second would require a chiral-breaking one. In momentum-space notation, where the cutoff is denoted by Λ,

$$C_0(\Lambda) + m_\pi^2 C_2^{(qm)}(\Lambda) = \frac{4\pi}{6m_N\Lambda}\left[(2n+1)^2\frac{\pi^2}{2} + \frac{m_\pi^2}{M_{NN}\Lambda}\log\left(\frac{\Lambda_*}{\Lambda}\right)\right]. \qquad 50.$$

Although the logarithmic divergence is suppressed by a power of Λ compared with the first term, it is a true divergence in physical quantities that must be renormalized at LO in Weinberg power counting. The $C_2^{(qm)}$ operator, which is formally subleading, must be promoted to LO if the full OPE is iterated, in agreement with the perturbative argument of Reference (23). On the other hand, the $C_2^{(qm)}$ contribution is numerically small (see dotted curve in the left panel of Figure 12, which neglects the Λ^{-2} corrections to the running). This smallness explains why Weinberg's power counting has been found to work well in this channel over a moderate range of cutoffs (9, 70, 75–78).

A possible conclusion is that OPE and the $O(m_q)$ LECs contribute to any amplitude at the same order in the expansion, and this is what leads to KSW power counting. However, a more general conclusion is that the difference between the OPE contribution for $m_q \neq 0$ and the OPE contribution in the chiral limit must

occur at the same order as the $O(m_q)$ counterterms. In many cases these two conclusions yield identical amplitudes, but not in the ${}^3S_1 - {}^3D_1$ channel.

In the ${}^3S_1 - {}^3D_1$ channel, in addition to the long-distance Yukawa interaction and the contact interaction, there is a strong tensor component of OPE that couples S and D waves. At distances $r \ll 1/m_\pi$, the central potential is negligible, and in the region $R < r \ll 1/M_{NN}$, we can neglect the angular-momentum barrier. Moreover, for $\sqrt{m_N E} \ll M_{NN}$, the total energy E can be treated as a perturbation. In this short-distance limit, we can keep only the chiral limit of the tensor force, and the Schrödinger equation can be diagonalized and solved exactly. In the diagonal basis, the Schrödinger equation decouples into an attractive singular potential and a repulsive potential. The solution for the attractive singular potential is a linear combination of Bessel functions (80, 84), and the wave function at this order is

$$u(r) = Ar^{3/4} \cos\left(\sqrt{\frac{6}{M_{NN} r}} + \phi_0\right), \qquad 51.$$

where A is a dimensionful normalization constant and ϕ_0 is the asymptotic phase, which determines the triplet scattering length. This solution oscillates ever faster as it approaches the origin, just as in Figure 11. As before, the issue is whether a $V_0(R)$ can be found such that the asymptotic phase ϕ_0 becomes R-independent. Matching logarithmic derivatives of the interior square-well and exterior attractive solutions at $r = R$ yields an equation whose solution is shown in the right panel of Figure 12. The renormalization-group flow is multi-branched and nonanalytic in g_A^2/f_π^2.

The LO phase shifts are indeed found to be cutoff independent (83), in agreement with the numerical analyses of References (84) and (77). As an example, the ${}^3S_1$ phase shift is shown in Figure 13. In these channels, the perturbative argument (69) is misleading; Weinberg's power counting does not seem to be formally inconsistent.

It was conjectured (83) that a formally consistent expansion in the pionful EFT is an expansion around the chiral limit. This expansion is equivalent to KSW power counting in the ${}^1S_0$ channel and equivalent to Weinberg power counting in the ${}^3S_1 - {}^3D_1$ coupled channels, i.e., it selects only the desirable features of both power countings. The LO potential $V(r;0)$, to be treated exactly, consists of the chirally symmetric component of OPE and nonderivative contact interactions. Deviations from the chiral limit $V(r;m_\pi) - V(r;0)$ can be treated perturbatively in all channels, and in fact, such a perturbative expansion is required in the ${}^1S_0$ channel but not in the ${}^3S_1 - {}^3D_1$ channel. Evidence was presented that this expansion converges, albeit slowly. The slowness is due not to the long-range pion physics itself, but to the fine-tuned short-distance physics [as argued previously (85)].

Although existing obstacles to a derivative and pion-mass expansion were removed, higher orders must be studied before the issue can be considered settled. For example (86), an incomplete subleading calculation with nonperturbative pions has found limits in fitting the effective range. Note also that alternative views

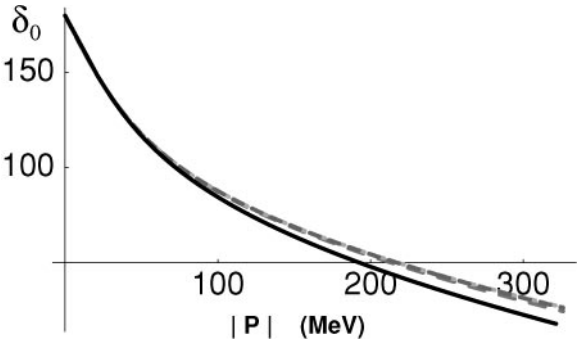

Figure 13 $^3S_1$ *NN* phase shift in LO in the EFT with nonperturbative pions, as a function of the center-of-mass momentum. The long-dashed, medium-dashed, and short-dashed lines have, respectively, R = 0.45 fm (Λ = 438 MeV), R = 0.21 fm (Λ = 938 MeV), and R = 0.10 fm (Λ = 1970 MeV). The solid line is the Nijmegen phase-shift analysis. (From Reference (83) with permission from Elsevier Science.)

of the renormalization of the pion ladder exist (87). Finally, there is an interesting suggestion of expanding the *NN* amplitude in the energy region where the *S*-wave phase shifts vanish (88). The connection between this expansion and the low-energy expansion described here has not been fully analyzed.

3.2.3. POTENTIALS AND FITS TO *NN* DATA Conceptually and numerically, the picture that emerges from the previous section is close to Weinberg's original proposal. To be formally consistent, we should expand the potential in powers of the pion mass. If we resum the effects of the pion mass in pion exchange, which can be done with higher-order error, then the LO potential becomes the same as in Weinberg's power counting. Corrections to the LO potential need not be iterated to all orders. Yet, as has been shown explicitly in the pionless EFT (14), they can be iterated with small error if one uses a regularization with a cutoff $\Lambda \sim M_{\rm QCD}$. Clearly, a potential that is correct up to a certain order ensures that the amplitude is correct to the same order.

Much work has been done in developing an EFT potential based on Weinberg's power counting. Traditionally, potential models have been plagued by problems of principle, such as the form of meson-nucleon interactions (e.g., pseudoscalar versus pseudovector pion coupling), renormalization issues, absence of a small expansion parameter, etc. Because the EFT potential explicitly includes only the exchange of pions, all these problems can be resolved. For any given choice of pion field, the form of interactions is fixed by the pattern of chiral symmetry breaking. Renormalization can be performed because all interactions consistent with symmetries are included. And the power counting (Equation 41) for the EFT potential implies that diagrams with an increasing number of loops *L*—and, in particular, with an increasing number of exchanged pions—should be progressively

less important. The EFT potential can be considered, in an average sense, a low-energy approximation to standard potential models.

In LO, $\nu = \nu_{\min} = 0$, the *NN* potential consists of simply static OPE and momentum-independent contact terms. This is obviously a very crude approximation to the *NN* potential; it is known that the nuclear force has other sizable components, such as a spin-orbit force, a strong short-range repulsion, and an intermediate range attraction. These are all generated in the next orders: $\nu = \nu_{\min} + 1$ corrections vanish owing to parity and time-reversal invariance, but several $\nu = \nu_{\min} + 2$ corrections remain. First, there are short-range corrections; they come from one-loop pion dressing of the lowest-order contact interactions and from $4N$ contact interactions with two derivatives or two powers of the pion mass. It is easy to show that the result of loop diagrams amounts to a simple shift of the contact parameters. Second, there are corrections to OPE; these come from vertex dressing and from recoil upon pion emission. Third, there are two-pion exchange (TPE) diagrams built out of the lowest-order πNN (and $\pi N\Delta$) interaction. At $\nu = \nu_{\min} + 3$, a few more TPE diagrams appear, which involve the $\pi\pi NN$ seagull vertices from the $\Delta = 1$ Lagrangian. To this order, there are also some small relativistic corrections. At $\nu = \nu_{\min} + 4$, a host of two-loop diagrams and new contact interactions emerge, and so on. Some diagrams are shown in Figure 14.

A calculation of all contributions to the *NN* potential up to $\nu = \nu_{\min} + 3$ was carried out (7, 9) using time-ordered perturbation theory. This EFT potential is energy-dependent, but equivalent potentials can be obtained through unitary transformations. An energy-independent potential is more convenient in many situations; the corresponding version has been derived (89).

The potential to this order has all the spin-isospin structure of phenomenological models, but its profile is determined by explicit degrees of freedom, symmetries, and power counting. The power counting suggests a hierarchy of short-range effects: *S* waves should depend strongly on the short-range parameters $C_0^{(S,T)}$; contact interactions affect *P*-wave phase shifts only in subleading order, so their effect should be smaller and approximately linear; and *D* and higher waves are directly affected by contact interactions at higher orders, being thus essentially determined by pion exchange. Whereas phenomenological potentials such as that in Reference (90) have similar short- and long-range structure, it is on TPE that chiral symmetry is particular influential. The chiral TPE, first derived in Reference (7) in the limit of a heavy Δ, was studied in detail (73). More recently, the chiral TPE potential was substituted for one-boson exchange in a Nijmegen phase-shift reanalysis of proton-proton data below 350 MeV (91), and a drop in χ^2 was observed. A new full Nijmegen phase-shift analysis is in the works, in which chiral TPE is used in the long-range potential (91).

Fits to *NN* phase shifts were done to this order with (9) and without (78) explicit Δ degrees of freedom. Although OPE and TPE diagrams are completely determined by LECs accessible in πN reactions, most of these LECs were not known at the time of Reference (9) and were also searched in the fit. Epelbaum et al. (78) took these parameters from a fit to πN scattering, which allowed for a simpler,

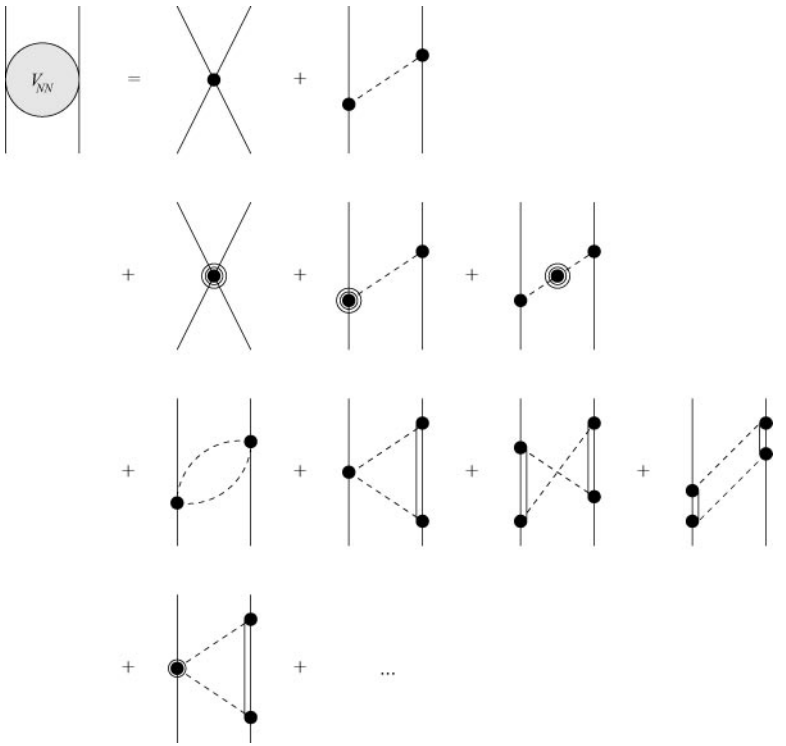

Figure 14 Some time-ordered diagrams that contribute to the *NN* potential in the pionful EFT. Solid lines represent nucleons; double lines, Δ; dashed lines, pions; dot, an interaction in $\mathcal{L}^{(0)}$; dot within circle, an interaction in $\mathcal{L}^{(1)}$; dot within two circles, an interaction in $\mathcal{L}^{(2)}$. The first line corresponds to $\nu = \nu_{\min}$, the second and third lines to $\nu = \nu_{\min} + 2$, the fourth line to $\nu = \nu_{\min} + 3$, and "..." denotes $\nu \geq \nu_{\min} + 4$. All orderings with at least one pion (or Δ) in intermediate states are included. Not shown are diagrams that contribute only to renormalization of parameters.

partial-wave-by-partial-wave fit of *NN* phase shifts. They found reasonable agreement with existing phase-shift analyses and deuteron properties. As an example, the $^3S_1$ phase shift at various orders is shown in Figure 15 and compared to the Nijmegen phase-shift analysis (26) (see Figures 2, 10, and 13). The contributions from the short-range parameters in this fit turn out to be similar to those from heavier resonances in phenomenological models (92).

Although the fits to $\nu = \nu_{\min} + 3$ are good, they are inferior to the so-called realistic potentials that use 40–50 parameters to fit data up to 300 MeV with a χ^2/d.o.f. near 1. First steps are being made to extend the EFT potential to $\nu = \nu_{\min} + 4$ (93–95). The results are promising, achieving quality comparable to realistic potentials. [Indeed, the difference among realistic potentials arises from

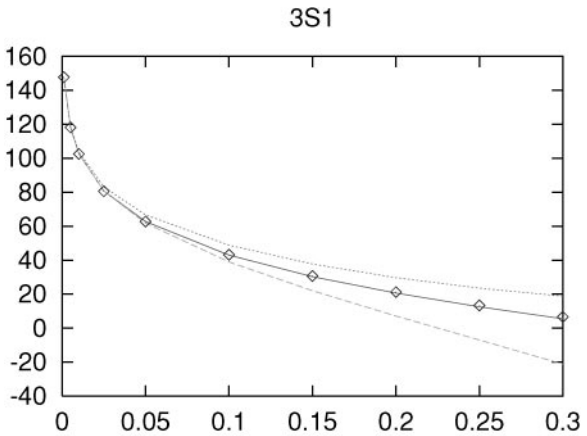

Figure 15 ${}^3S_1$ *NN* phase shift (in degrees) in the EFT with Weinberg counting, as a function of the lab energy (in GeV). The dotted, dashed, and solid lines are the results at orders $\nu = \nu_{\min}$, $\nu = \nu_{\min} + 2$, and $\nu = \nu_{\min} + 3$, respectively. The squares are the Nijmegen phase-shift analysis. (From Reference (78), courtesy of U.-G. Meißner.)

high-momentum intermediate states probing scales that cannot be uniquely fixed by low-energy fits (96).]

3.2.4. ISOSPIN VIOLATION The mass difference between u and d quarks breaks isospin symmetry explicitly. The meson masses indicate that the ratio $\varepsilon \equiv (m_u - m_d)/(m_u + m_d) \sim 1/3$. Naively, this suggests that isospin might not be a much better symmetry than the rest of the chiral group. On the other hand, a cursory look at hadron masses and a more complete analysis of dynamical amplitudes show that isospin is typically broken only at the few-percent level.

Why is isospin such a good symmetry at low energies? The answer can be found in the pattern of chiral-symmetry breaking incorporated in the chiral Lagrangian (11). Explicit chiral-symmetry-breaking effects are present already at index $\Delta = 0$ through the pion mass term, but operators generated by the quark mass difference appear only at $\Delta = 1$ through a term that contributes to the nucleon mass splitting and—because of chiral symmetry—to certain pion-nucleon interactions. As a consequence, in most quantities, isospin breaking competes with isospin-conserving operators of lower order, and its relative size is not ε but $\varepsilon(Q/M_{\rm QCD})^n$, where n is a positive integer. In other words, isospin is an accidental symmetry (11): a symmetry of the lowest-order EFT that is not a symmetry of the underlying theory. The only known exception to this rule is in the isoscalar t channel in πN scattering at threshold, where there is no contribution from the $\Delta = 0$ Lagrangian, and both the isospin-conserving and -violating amplitudes start at the same order. The isospin-violating piece comes from the pion-nucleon interactions linked to the nucleon mass splitting. Unfortunately, this is hard to see experimentally.

Along these lines, one can study the expected size of isospin breaking in the nuclear potential. We follow the standard nomenclature, in which an isospin-symmetric potential is "class I," a potential that breaks charge independence but not charge symmetry—defined as a rotation of π around the 2-axis in isospin space—is "class II," a potential that breaks charge symmetry but vanishes in the *np* system is "class III," and a potential that breaks charge symmetry but causes mixing in the *np* system is "class IV."

At $Q \sim M_{NN}$, photon exchanges are perturbative. These standard electromagnetic effects from "soft" photons can be obtained straightforwardly from gauge-invariant operators that involve the photon field. In addition, isospin violation arises from the quark masses, from indirect electromagnetic effects, and from simultaneous pion-photon exchange. In order to compare the various sources of isospin breaking, we note that the size of electromagnetic effects in loops is typically $\sim\alpha/\pi$ which, numerically, is $\sim\varepsilon(Q/M_{\rm QCD})^3$.

The leading isospin-breaking interactions in Weinberg's power counting have been derived (11). (The necessary modification of Weinberg's counting discussed in Section 3.2.2 shows that chiral-symmetry-breaking terms are even more suppressed than chiral-symmetric ones. This modification is not expected to affect the relative sizes among isospin-breaking interactions.) No isospin-violating effects appear at LO, $\nu = \nu_{\rm min}$, so the leading potential is class I. The first isospin-breaking effect (in addition to Coulomb exchange) appears at $\nu = \nu_{\rm min} + 1$ in the form of a class II isospin violation from the pion mass splitting $[\Delta m_\pi^2 = O(\alpha M_{\rm QCD}^2/\pi)]$ in OPE. One order down, $\nu = \nu_{\rm min} + 2$, a class III force appears mainly from the quark mass difference through breaking in the πNN coupling $[\beta_1 = O(\varepsilon m_\pi^2/M_{\rm QCD}^2)]$ in OPE, from contact terms $[\gamma_{s,\sigma} = O(\varepsilon m_\pi^2/M_{\rm QCD}^4)]$, and from the nucleon mass difference $[\Delta m_N = O(\varepsilon m_\pi^2/M_{\rm QCD})]$. To this order, the isospin-violating nuclear potential is an *NN* potential of the form

$$V_{ib} = V_{\rm II}\left[(t_1)_3(t_2)_3 - \boldsymbol{t}_1 \cdot \boldsymbol{t}_2\right] + V_{\rm III}\left[(t_1)_3 + (t_2)_3\right], \tag{52.}$$

where

$$V_{\rm II} = -\left(\frac{g_A}{f_\pi}\right)^2 \frac{\vec{q}\cdot\vec{\sigma}_1\vec{q}\cdot\vec{\sigma}_2}{\left(\vec{q}^2 + m_{\pi^0}^2\right)\left(\vec{q}^2 + m_{\pi^\pm}^2\right)}\left(\Delta m_\pi^2 + \Delta m_N^2\right), \tag{53.}$$

$$V_{\rm III} = \frac{g_A\beta_1}{2f_\pi^2}\frac{\vec{q}\cdot\vec{\sigma}_1\vec{q}\cdot\vec{\sigma}_2}{\vec{q}^2 + m_\pi^2} - \left(\gamma_s + \gamma_\sigma\vec{\sigma}_1\cdot\vec{\sigma}_2\right). \tag{54.}$$

Finally, class IV forces appear only at order $\nu = \nu_{\rm min} + 3$.

We conclude that the pattern of symmetry breaking in QCD naturally suggests a hierarchy of classes in the nuclear potential (11):

$$\frac{\langle V_{\rm M+I}\rangle}{\langle V_{\rm M}\rangle} \sim O\left(\frac{Q}{M_{\rm QCD}}\right), \tag{55.}$$

where $\langle V_{\rm M}\rangle$ denotes the average contribution of the leading class-M potential.

This qualitatively explains not only why isospin is a good approximate symmetry at low energies, but also why charge symmetry is an even better symmetry. It gives, for example, the observed isospin structure of the Coulomb-corrected scattering lengths (97), $a_{np} \simeq 4 \times [(a_{nn} + a_{pp})/2 - a_{np}] \simeq 4^2 \times (a_{pp} - a_{nn})$.

One can use the above formalism to do consistent and systematic calculations of isospin violation. For example, the isospin-violating potential of ranges $\sim 1/m_\pi$ and $\sim 1/2m_\pi$ up to $\nu = \nu_{\min} + 3$ were computed (98–100). In contrast to previous attempts that lacked an EFT framework, the EFT results are invariant under both gauge transformations and pion-field redefinitions and have simple forms. The component of range $\sim 1/m_\pi$ comes from diagrams with all possible one-photon dressings of OPE, plus the relevant counterterms (98). Its isospin structure allows only charged-pion exchange and therefore is class II. This $\pi\gamma$ potential has been incorporated in a Nijmegen phase shift reanalysis of *np* data below 350 MeV (98). We can use the values for the πNN coupling constants determined by the analysis to find that their isospin breaking (β_1) is consistent with zero, with an uncertainty comparable to our expectation from dimensional analysis and from $\pi-\eta-\eta'$ mixing (101). Similarly, the two contact interactions ($\gamma_{s,t}$) might be viewed as originating in $\rho-\omega$ mixing and pseudovector-meson exchange (in particular close-lying doublets such as a_1-f_1) (101, 102). The components of range $\sim 1/2m_\pi$ come from two sources. One is the pion mass difference (Δm_π^2) in TPE that generates a class II potential (99); the other is a $\pi\pi NN$ seagull that arises as a chiral partner of the nucleon mass difference (Δm_N) and produces a class III TPE potential (100). All these effects are relatively small, with estimated contributions to the scattering lengths of approximately ± 0.5 fm.

Walzl et al. (103) carried out a fit to *NN* phase shifts that included various of the above isospin-breaking interactions, improving on an earlier analysis with perturbative pions (104). Isospin breaking in the scattering lengths can be accommodated, and higher energies and partial waves can be predicted. A next-order calculation should achieve the level of precision of modern phenomenological potentials.

3.3. Three- and Four-Nucleon Systems

Few-body systems raise the issue of few-body forces allowed by symmetries, which will at some level contribute to observables. One of the advantages of an EFT framework is the possibility of deriving consistent few-body forces, free of off-shell ambiguities. In the standard nuclear physics approach, few-nucleon forces are either inspired by arguments that are independent of the assumptions invoked in the *NN* potential, or are simply guessed at on phenomenological terms.

The pionful EFT offers some insight into few-nucleon forces. In addition to contact interactions as in the pionless theory, it has further pion-exchange components. The potential, defined as a sub-amplitude, includes (for $A > 2$) diagrams that have $C \geq 1$ separately connected pieces. An *n*-nucleon force is a contribution to the potential that connects *n* nucleons.

Weinberg's power counting, embodied in Equation 41, suggests a hierarchy of few-nucleon forces. As in the *NN* case, this power counting relies on an implicit assumption about the scale in contact interactions. We saw in Section 2.2.2 that, in the pionless EFT, the running of the renormalization group toward low energies enhances the size of three-body forces. The latter get contaminated by the fine-tuning present in the two-body sector. Whether the same happens at the higher energies relevant to the pionful theory is not clear. A portion of the 3*N* forces in the pionless theory matches onto diagrams of the pionful theory that are the iteration of the *NN* potential through *NN* intermediate states where at least one nucleon has momentum $O(m_\pi)$. It is conceivable that the enhancement is removed from contact interactions once the EFT is extended to momenta of $O(m_\pi)$.

The new forces that appear in systems with more than two nucleons have been derived (7, 8, 10). The dominant potential, at $\nu = 6 - 3A = \nu_{\min}$, is simply the *NN* potential of lowest order, which we encountered in Section 3.2.3. We can easily verify that, if the Δ is kept as an explicit degree of freedom, a 3*N* potential will arise at $\nu = \nu_{\min} + 2$, a 4*N* potential at $\nu = \nu_{\min} + 4$, and so on. Approximate chiral symmetry implies that *n*-nucleon forces V_{nN} obey a hierarchy of the type

$$\frac{\langle V_{(n+1)N}\rangle}{\langle V_{nN}\rangle} \sim O\left(\frac{Q}{M_{\rm QCD}}\right)^2, \qquad 56.$$

with $\langle V_{nN}\rangle$ denoting the contribution per *n*-plet. (This hierarchy is a nontrivial consequence of chiral symmetry; some nonchiral models produce large three-body forces.) As discussed in Section 3.2.2, we expect $|\langle V_{2N}\rangle| \sim 10$ MeV. Using m_π and m_ρ for Q and $M_{\rm QCD}$, respectively, the suppression factor is $\sim$0.05, give or take a factor of two or three. These estimates are in accord with detailed few-nucleon phenomenology based on potentials that include small 3*N* and no 4*N* forces. This is shown in Table 1 in the case of the AV18/IL2 potential (105).

It proves instructive to look at the form of the first few terms in the few-nucleon potential. At $\nu = \nu_{\min} + 2$, in addition to corrections to the *NN* potential, one also finds diagrams that involve either three nucleons or two pairs of nucleons

TABLE 1 Contributions of the two-, three- and four-nucleon potentials (per doublet, per triplet, and per quadruplet, respectively): Weinberg power counting (W pc) and calculations (105) with the AV18/IL2 potential for the ground states of various light nuclei (^{2}H, ^{3}H, etc.)

(MeV)	**W pc**	**^{2}H**	**^{3}H**	**^{4}He**	**^{6}He**	**^{7}Li**	**^{8}Be**	**^{9}Be**	**^{10}B**
$\lvert\langle V_{2N}\rangle\rvert$	$\sim$10	22	20	23	13	11	11	9.4	8.9
$\lvert\langle V_{3N}\rangle\rvert$	$\sim$0.5	—	1.5	2.1	0.55	0.43	0.38	0.29	0.30
$\lvert\langle V_{4N}\rangle\rvert$	$\sim$0.02	—	—	?	?	?	?	?	?
$\frac{\lvert\langle V_{3N}\rangle\rvert}{\lvert\langle V_{2N}\rangle\rvert}$	$\sim$0.05	—	0.075	0.091	0.042	0.039	0.035	0.031	0.034
$\frac{\lvert\langle V_{4N}\rangle\rvert}{\lvert\langle V_{3N}\rangle\rvert}$	$\sim$0.05	—	—	?	?	?	?	?	?

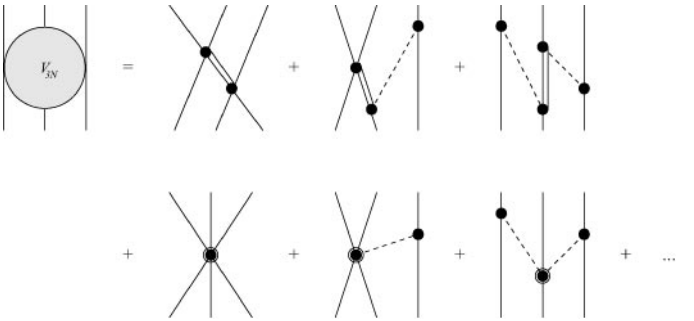

Figure 16 Some time-ordered diagrams that contribute to the three-nucleon potential in the pionful EFT. Solid lines represent nucleons; double lines, Δ; dashed lines, pions; heavy dot, an interaction in $\mathcal{L}^{(0)}$; dot within a circle, an interaction in $\mathcal{L}^{(1)}$. The first line corresponds to $\nu = \nu_{\min} + 2$, the second line to $\nu = \nu_{\min} + 3$, and "..." denotes $\nu \geq \nu_{\min} + 4$. All nucleon permutations and orderings with at least one pion or Δ in intermediate states are included.

connected via leading contact interactions and static pions. The various orderings of these diagrams cancel among themselves and against contributions from the energy-dependent piece of the iterated *NN* potential that appears at the same order (6, 8, 10). Alternatively, redefining the potential to eliminate energy dependence leads to no 3*N* TPE forces of this type at all (89). The only 3*N* forces that remain to this order are generated by the Δ isobar, if the Δ is kept explicit in the EFT. At $\nu_{\min} + 3$, further terms with similar structure arise (10, 11) (see Figure 16).

If, instead, the Δ is integrated out, its contributions appear through the parameters of the potential at $\nu = \nu_{\min} + 3$. In this case, there are no 3*N* forces up to $\nu = \nu_{\min} + 3$. Epelbaum et al. (106) used the $\nu = \nu_{\min} + 2$ deltaless potential of Reference (78) to predict properties of the 3*N* and 4*N* systems. The small variation allowed in the cutoff does not permit firm conclusions about consistency in renormalization. Low-energy 3*N* scattering observables and 3*N* and 4*N* binding energies come out similar to conventional-potential results. An "A_y puzzle" plagues conventional models: All potentials that fit *NN* data well fall short of reproducing the elastic neutron analyzing power, A_y, at energies as low as 3 MeV. This seems to be the case with chiral potentials as well (107).

The leading 3*N* potential (10) has components with three different ranges: TPE, OPE/short-range, and purely short-range. (Relativistic corrections neglected below are discussed in Reference (74).)

The TPE part of the potential is determined in terms of πN scattering observables (10). It is similar to the Tucson-Melbourne (TM) and Brazil potentials (108), but it corrects a deficiency of the TM potential in regard to chiral symmetry (109). The resulting TM′ potential has been studied in detail (110, 111). Hüber et al. (111) showed that one of the components of the force is dominant in 3*N* elastic scattering

observables. This explains why all existing TPE $3N$ forces give essentially the same results for the $3N$ continuum after being fitted to the triton energy. This type of $3N$ force does not much improve agreement for A_y (111).

The novel OPE/short-range components of the potential involve two $\pi(\bar{N}N)^2$ interactions of strengths not determined by chiral symmetry alone (10). These parameters can be thought of as representing short-range effects such as σ and ω exchanges with an intermediate $N(1440)$ resonance, and ρ exchange from a $\pi\rho$ Kroll-Ruderman term (112). Because of the antisymmetry of the wave function, only one combination of parameters contributes (I.W. Stewart, private communication; E. Epelbaum, private communication). This combination can be determined from reactions that involve only two nucleons, as discussed in Section 3.4 below. If this combination has natural size, this force, in conjunction with TM′, can bridge a significant part of the discrepancy between "realistic" NN potentials and A_y data (111).

The purely short-range components of the potential can be determined only from few-nucleon systems (10). As we have seen (Section 2.2), the Pauli principle leads to a single LEC. Once this LEC is determined from one $3N$ input (such as the triton binding energy), all other observables (such as A_y) can be predicted, once the OPE/short-range component has been fixed by data involving just two nucleons.

It is apparent that the pionful EFT brings new forces into play, and these new elements might resolve remaining issues in the description of data. This prospect calls for a fully consistent $\nu_{\min} + 3$ calculation with maximal NN input.

3.4. Processes with External Probes

The power counting arguments of Section 3.2.2 can be generalized to the case where external probes with momenta $Q \sim M_{NN}$ interact with few-nucleon systems. The probes deposit an energy $\sim M_{NN}$ onto the nuclear system, so that, if we define the kernel K as the sum of irreducible diagrams to which the probes are attached, the power counting (Equation 41) applies equally well to K. Interactions among nucleons that occur before or after scattering can be treated as before: Iteration of the potential gives rise to the wave function $|\psi\rangle$ ($|\psi'\rangle$) of the initial (final) nuclear state. The full scattering amplitude is then

$$T = \langle\psi'|K|\psi\rangle. \qquad 57.$$

The pionful EFT can also handle scattering at smaller Q, of course, but then Equations 41 and 57 must be modified. When the deposited energy is $\sim M_{NN}^2/m_N$—for example, when the incoming probes are photons of momenta $Q \sim M_{NN}^2/m_N$—there can be intermediate few-nucleon states that are reducible, and the breakdown of T into kernel and wave functions is more complicated (113). In this situation, a perturbative treatment of pions, or even better, the pionless EFT, should suffice.

In practice, it is frequently desirable to minimize nuclear wave-function errors by using a high-precision phenomenological potential. That this is a good approximation is suggested by a comparison (76) between a simplified version of the

EFT potential of Reference (9) and the Argonne V18 potential (90), which show agreement in most aspects of the wave function. The cost of this "hybrid approach" (8) is the introduction of an uncontrolled error due to a possible mismatch between the off-shell extensions of the kernel and the potential. This error can, however, be estimated by the use of several different phenomenological potentials of similar quality.

As with few-nucleon forces, the factor $-2C$ in Equation 41 implies that external probes tend to interact predominantly with a single nucleon, simultaneous interactions with more than one nucleon being suppressed by powers of $(Q/M_{\rm QCD})^2$. Again, this generic dominance of the impulse approximation is a well-known result that arises naturally here. This is of course what allows extraction, to a certain accuracy, of one-nucleon parameters from nuclear experiments. A valuable by-product of the EFT is to provide a consistent framework for one- and few-nucleon dynamics, whereby few-nucleon processes can be used to infer one-nucleon properties. More interesting from the purely nuclear-dynamics perspective, however, are processes in which the leading single-nucleon contribution vanishes with a particular choice of experimental conditions, for example the threshold region. In this case, certain *NN* contributions, especially in the relatively large deuteron, can become important. Further examination of the structure of the chiral Lagrangian reveals that *NN* contributions tend to be dominated by pion exchange. Indeed, photons and pions couple to $4N$ operators only at $O(Q/M_{\rm QCD})$ relative to pion-exchange diagrams constructed out of the LO Lagrangian. Thus, power counting justifies the "chiral filter hypothesis" that was put forward to summarize some empirical results on electroweak form factors (114). This "pion dominance" ensures that *NN* contributions from the EFT in lowest orders tend to be similar to those in phenomenological models that include pion-exchange currents.

Many processes have been analyzed in the pionful EFT. Some of those processes are extensions to higher energies of the same electroweak processes described in Section 2.1. For example,

- $ed \to ed$ and deuteron form factors (115)
- $\vec{e}d \to eNN$ and parity violation (116)
- $np \to d\gamma$ and meson-exchange currents (117)
- $\vec{n}p \to d\gamma$ and parity violation (118)
- $pp \to de^+\nu_e$ and axial currents (119)
- $p\,{}^3\mathrm{He} \to {}^4\mathrm{He}\,e^+\nu_e$ and solar neutrino production (120)
- $\nu d \to lNN$ and solar neutrino detection (121)
- $\mu d \to \nu_\mu nn$ and its measured rate (122)
- $\gamma d \to \gamma d$ and nucleon polarizabilities (113, 123)

For details, we refer the reader to more extensive reviews (18) and the original papers. Here we briefly discuss the processes most germane to the pionful theory, involving pions in initial and/or final states.

3.4.1. $\pi d \to \pi d$ This reaction offers perhaps the most direct way to check the consistency of EFT in one- and few-nucleon systems. For simplicity, consider the region near threshold with the Δ integrated out. There the lowest-order, $\nu = \nu_{\min} = -2$ contributions to the kernel vanish because the pion is in an s wave and the target is isoscalar. The $\nu = \nu_{\min} + 1$ term comes from the (small) isoscalar pion-nucleon seagull, related in lowest order to the pion-nucleon isoscalar amplitude $b^{(0)}$. The $\nu = \nu_{\min} + 2$ contributions come from corrections to πN scattering and NN diagrams, which involve not only $b^{(0)}$ but also the much larger isovector amplitude $b^{(1)}$. These various contributions to the πd scattering length have been estimated (8, 124) and found to agree with previous, more phenomenological calculations, which have been used to extract $b^{(0)}$. Partial sets of higher-order corrections have been evaluated (125) (see Reference (126) for the related, double-charge-exchange process). A consistent $\nu = \nu_{\min} + 3$ calculation of πd elastic scattering is in progress (127). Eventually, a $\nu = \nu_{\min} + 4$ calculation might be required in order to determine the chiral-symmetry breaking LEC $C_2^{(qm)}$, discussed further below in connection with lattice QCD. Charge-symmetry-breaking effects were considered in Reference (128). An alternative approach with perturbative pions (129) also seems to accommodate the available experimental data.

3.4.2. $\gamma^{(*)}d \to \pi^0 d$ The reaction $\gamma^{(*)}d \to \pi^0 d$ offers the possibility to test a prediction arising from a combination of NN contributions and the single-neutron amplitude. The differential cross section for a photon of momentum k and longitudinal polarization ϵ_L to produce a pion of momentum q is, at threshold,

$$\left[\left(\frac{3k}{8q}\right)\left(\frac{d\sigma}{d\Omega}\right)\right]_{q=0} = |E_d|^2 + \epsilon_L |L_d|^2, \qquad 58.$$

where the electric dipole amplitude $E_d(k^2)$ characterizes the transverse response and $L_d(k^2)$ the longitudinal response.

$E_d(0)$ was studied up to $\nu = \nu_{\min} + 3$ with the Δ integrated out (130). Contributions are classified according to whether the external light particles interact with one or with both nucleons. The one-nucleon part of the kernel is given by standard $A = 1$ χPT, with due account of P waves and Fermi motion inside the deuteron. The neutrality of the outgoing s-wave pion ensures that the leading $\nu = -2 = \nu_{\min}$ terms vanish. The first NN part of the kernel appears at $\nu = \nu_{\min} + 2$; it comes from a virtual charged pion photoproduced on one nucleon that rescatters on the other nucleon with charge exchange. These contributions are actually numerically larger than indicated by power counting because of the relatively large deuteron size. Smaller NN terms appear at $\nu = \nu_{\min} + 3$ from corrections in either nucleon. Results for $E_d(0)$ up to $\nu = \nu_{\min} + 3$ (130) are shown in Table 2. They correspond to the Argonne V18 potential (90) and a cutoff $\Lambda = 1000$ MeV. Other realistic potentials and cutoffs from 650 to 1500 MeV give the same result within 5%. The chiral potentials of Section 3.2.3 are more cumbersome to use, but they yield results similar to those of other potentials. Two-nucleon contributions seem to be converging, although more convincing evidence would come from next order,

TABLE 2 Values for $E_d(0)$ in units of $10^{-3}/m_{\pi^+}$ from one-nucleon contributions (N) up to $\nu = \nu_{\min} + 3$, two-nucleon kernel (NN) at $\nu = \nu_{\min} + 2$ and at $\nu = \nu_{\min} + 3$, and their sum ($N + NN$)

N	NN		$N + NN$
$\nu \leq \nu_{\min} + 3$	$\nu = \nu_{\min} + 2$	$\nu = \nu_{\min} + 3$	$\nu \leq \nu_{\min} + 3$
0.36	−1.90	−0.25	−1.79

where loops appear. A model-dependent estimate (131) of some $\nu = \nu_{\min}+4$ terms suggests a 10% or larger error from neglected higher orders in the kernel itself. The single-scattering contribution depends on the amplitude for $\gamma n \to \pi^0 n$, $E_{0+}^{(\pi^0 n)}$, in such a way that $E_d(0) \sim -1.79 - 0.38(2.13 - E_{0+}^{(\pi^0 n)})$ in units of $10^{-3}/m_{\pi^+}$. Thus, sensitivity to $E_{0+}^{(\pi^0 n)}$ survives the large NN contribution at $\nu = \nu_{\min} + 2$.

We see that working within the EFT yields a testable prediction, $E_d(0) = -(1.8 \pm 0.2) \cdot 10^{-3}/m_{\pi^+}$ (130). It is remarkable that, for this process, EFT results differ significantly from tree-level models of the type traditionally used in nuclear physics. For example, the models in Reference (132) predict the threshold cross section to be about twice as large as predicted by EFT. Most of the difference comes from one-nucleon loop diagrams; tree-level models tend to differ from χPT mostly by having a smaller $E_{0+}^{(\pi^0 n)}$, which increases $|E_d|$. A test of this prediction—an important check of our understanding of the role of QCD at low energies—was carried out at Saskatoon (133). Figure 17 shows the experimental results for the pion photoproduction cross section near threshold, along with the EFT prediction at threshold (130). Estimated inelastic contributions (133, 134) are smaller than 10% throughout the range of energies shown. At threshold, Reference (133) finds $E_d(0) = -(1.45 \pm 0.09) \cdot 10^{-3}/m_{\pi^+}$. Although agreement with the EFT to order $\nu = \nu_{\min} + 3$ is not better than a reasonable estimate of higher-order terms, it is clearly superior to tree-level models. This is compelling evidence of chiral loops.

A further test of the EFT comes from the coherent neutral-pion electroproduction on the deuteron. $E_d(k^2)$ and $L_d(k^2)$ were predicted to $\nu = \nu_{\min} + 2$ (with no new free parameters) (135), for momentum transfer in the range 0–0.1 GeV^2. Because $E_{0+}^{(\pi^0 p)}$ is not well-reproduced at this order, only the k^2 dependence can be tested. This reaction was measured at $k^2 = -0.1$ GeV^2 in Mainz (136), and values for $|E_d(-0.1)|$ and $|L_d(-0.1)|$ were extracted. If they are compared with the results from Reference (135) simply shifted by a k^2-independent amount in order to reproduce the $E_d(0)$ of the $\nu = \nu_{\min} + 3$ calculation, then there is good agreement for $|E_d(-0.1)|$, but $|L_d(-0.1)|$ fails by a factor of two (136). Because the calculated $L_d(k^2)$ is not dominated by a single mechanism to the extent $E_d(k^2)$ is, it is possible that it suffers from stronger corrections in next order. An extension of these calculations to higher order and beyond threshold is highly desirable.

3.4.3. *$NN \to NN\pi$* The reaction $NN \to NN\pi$ has attracted great interest because standard phenomenological mechanisms fail to reproduce the small cross section

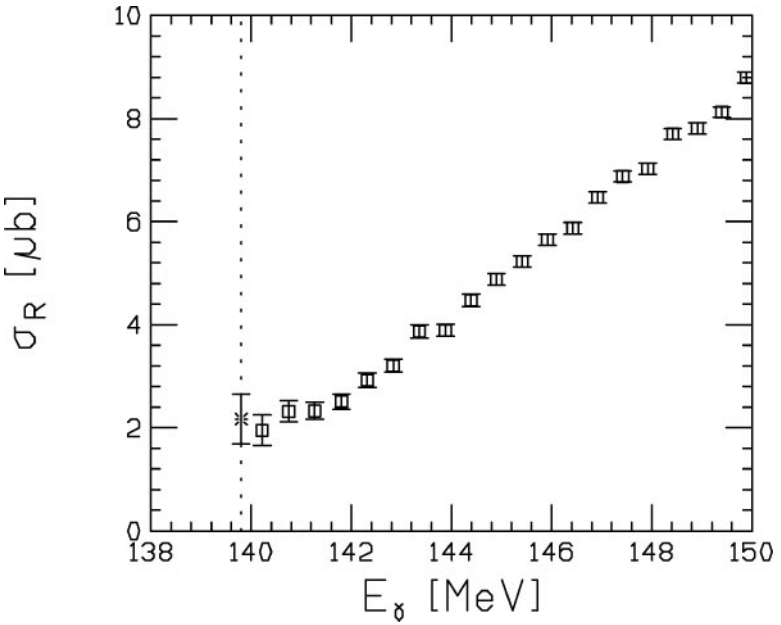

Figure 17 Reduced cross section $\sigma_R = (k/q)\sigma$ for neutral-pion photoproduction as a function of the photon energy. Threshold is marked by a dotted line. The star at threshold is the EFT prediction (130), and squares are data points (133). (Figure courtesy of U.-G. Meißner.)

observed near threshold. This reaction involves larger momenta of $O(\sqrt{m_\pi m_N})$, so the relevant expansion parameter here is not so small, $(m_\pi/m_N)^{\frac{1}{2}}$. This process is therefore not a good testing ground for EFT ideas. But $(m_\pi/m_N)^{\frac{1}{2}}$ is still <1, so at least in some formal sense we can perform a low-energy expansion. In References (137) and (138), the chiral expansion was adapted to this reaction and the first few contributions were estimated. [Note that—contrary to what is stated in Reference (139)—momenta $\sim\sqrt{m_\pi m_N}$ do not necessarily imply a breakdown of the nonrelativistic expansion, since $p^4/m_N^3 \sim (m_\pi/m_N)(p^2/m_N)$ is still small.]

Initial attention concentrated on $pp \to pp\pi^0$ at threshold. The lowest-order terms all vanish, and the formally leading nonvanishing terms—an impulse term and a similar diagram from the Δ isobar—are anomalously small and partly cancel. Accordingly, the bulk of the cross section must arise from contributions that are relatively unimportant in other processes: isoscalar pion rescattering, TPE, and high-order short-range $\pi(\bar{N}N)^2$ terms. Whereas the first two contributions are calculable, the third involves LECs that can only be fitted or modeled. These LECs can be thought of as originating from heavier-meson exchange: pair diagrams with σ and ω exchange, and a $\pi\rho\omega$ coupling, among other, smaller terms (140). Van Kolck et al. (140) showed that a large uncertainty comes from the short-range

features of the wave function, so a more systematic study awaits the development of chiral potentials that are accurate at the relevant energies. Other EFT studies of this channel, including attempts to compute TPE, can be found in Reference (141).

More problematic is the situation with the threshold cross section of the less-suppressed channels $NN \to d\pi$ and $\to pn\pi$. In those channels, the Weinberg-Tomozawa $\pi\pi NN$ term, fixed by chiral symmetry, dominates. Wave-function dependence is much smaller, yet a calculation that includes leading and some subleading contributions underpredicts the data by a factor of $\sim$2 (142). A calculation that includes TPE is badly needed.

Despite these problems, much can be learned from this reaction in the threshold region. One example is charge-symmetry breaking. The nucleon mass splitting comes from both the quark-mass-difference and electromagnetic effects, $\Delta m_N = \delta m_N + \bar{\delta} m_N$, with $\delta m_N = O(\varepsilon m_\pi^2/M_{\rm QCD})$ and $\bar{\delta} m_N = O(\alpha M_{\rm QCD}/\pi)$. Determining the two LECs δm_N and $\bar{\delta} m_N$ separately is interesting for several reasons: Coupled to a lattice evaluation of δm_N, it can be used to extract quark masses; it can test quark models that evaluate $\bar{\delta} m_N$; and it can constrain a possible time variation of α because ^{4}He nucleosynthesis is sensitive to Δm_N. These LECs contribute in combinations other than Δm_N to processes involving pions because the two operators that generate the nucleon mass difference have different chiral partners, which involve an even number of pions. Unfortunately, these LECs are hard to measure directly in πN scattering. The forward-backward asymmetry in $np \to d\pi^0$, on the other hand, is sensitive to the charge-symmetry breaking from these operators, and it has been calculated (143). Because the asymmetry is related to a ratio of amplitudes, some of the uncertainties in the strong-interaction physics are reduced. The asymmetry is being measured at TRIUMF (144), at a level that could allow for an observation of the quark-mass-difference effect. A related experiment, $dd \to \alpha\pi^0$, which can address the same issues but with different theoretical uncertainties, has been proposed at the Indiana University Cyclotron Facility (IUCF) (145).

It is possible that some of the problems encountered at threshold stem from the smallness of pion s waves, which show poor convergence also in $A = 1$ χPT—for example, in neutral pion photoproduction on the proton. Indeed, p-wave pion production seems better behaved. Reference (138) calculates the first two orders of the cross section for the $pp \to pp\pi^0$ reaction with initial nucleons in the spin $S = 1$ state in the direction of the incoming center-of-mass momentum, as a function of the outgoing pion momentum in the range 0.5–1 m_π. With no free parameters, good convergence and reasonable agreement with data are found. It was also pointed out that other observables would, at that order, be sensitive to a combination of $\pi(\bar{N}N)^2$ LECs that affects the leading $3N$ force, discussed in Section 3.3. In particular, the amplitude for the $^1S_0 \to (^3S_1 - {}^3D_1)p$ transition, which vanishes in LO, is very sensitive to this LEC. This amplitude, extracted from the $pp \to pn\pi^+$ data for pion momenta in the range 0.2–0.5 m_π, can be fitted quite well with a natural-sized LEC (138). This value for the LEC can be used in the $3N$ potential to improve the predictive power of the chiral potential.

All calculations of pion-production observables have involved approximations necessary to match the kernel and wave functions. A critical discussion of these approximations can be found in Reference (146). Issues such as the size of the contribution of the πNN cut, not well accounted for in the common approximations, need to be better understood. Pion production is wide open for further development.

3.5. Connection with Lattice QCD

How can we deduce nuclear physics from QCD? As we have seen, light nuclei are large objects of size $\sim 1/M_{NN} \gg 1/M_{\rm QCD}$ or larger. Dynamics at this scale can be understood within the EFT, and all nuclear information is encoded in the parameters of the EFT Lagrangian. These parameters, in turn, are fixed by the physics of smaller distances. If the EFT can somehow be matched onto QCD at some scale not far below $M_{\rm QCD}$, the EFT can be used to predict all of traditional nuclear physics. The EFT allows us to bridge the gap from the QCD Lagrangian to nuclear physics in two stages, according to the two energy scales.

At present, the best hope for a solution of QCD in the regime of large coupling constant relevant for nuclear physics is an explicit numerical solution on the lattice. However, the large size of nuclei makes their direct simulation practically and intellectually unsound. A more reasonable goal is to match lattice QCD with the EFT, which requires lattices not much larger than $1/M_{\rm QCD}$. We are still far from this goal, but a few steps have already been taken.

One obstacle arises from the difficulty in simulating small pion masses. For example, Reference (147) computes the ${}^1S_0$ and ${}^3S_1$ scattering lengths in quenched QCD with $m_\pi \gtrsim 500$ MeV.

The pion-mass dependence of nuclear forces comes in explicitly from pion propagators in pion exchange, and implicitly from short-range interactions. For illustration, Figure 18 exhibits the deuteron binding energy and the ${}^3S_1$ scattering

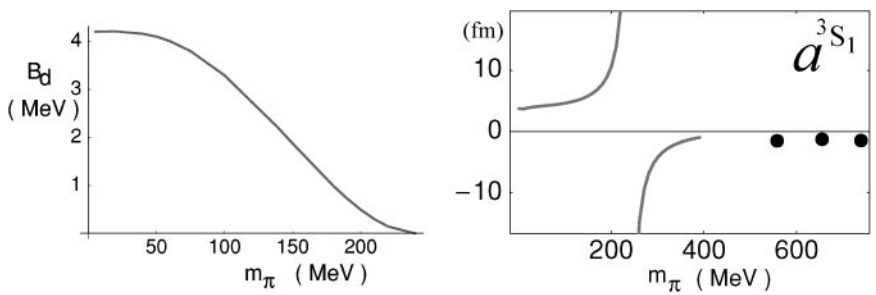

Figure 18 The deuteron binding energy (*left panel*) and the ${}^3S_1$ scattering length (*right panel*) as functions of the pion mass that explicitly appears in the OPE potential. Implicit pion-mass dependence was not calculated: Other parameters were set to their physical values for all m_π. The dots are quenched lattice QCD data. (From Reference (83) with permission from Elsevier Science.)

length that stem from the leading explicit m_π dependence in the expansion around the chiral limit (83). A higher-order two-derivative contact interaction was also included and fitted to the triplet effective range. For the physical value of the pion mass, one gets the deuteron binding energy to reasonable accuracy, $B_d = 2.211$ MeV (essentially independent of the cutoff R). In the chiral limit, the deuteron is bound by $B_d^0 \simeq 4.2$ MeV. This value is still somewhat small compared with $f_\pi^2/2m_N \sim 10$ MeV, which one might expect to arise in QCD, and therefore one would conclude that the deuteron is still weakly bound in the chiral limit! This calculation of the explicit m_π dependence agrees with that obtained with the AV18 potential (R. Wiringa, private communication) with $m_\pi = 0$, namely $B_d^{0(AV18)} \simeq 4.1$ MeV. Figure 18 also shows the lattice data for the triplet scattering length from Reference (147).

Phenomenological models typically can only vary m_π in OPE, but all aspects of m_π dependence can in principle be determined in the pionful EFT. Since the pion mass can be varied up to $M_{\rm QCD}$, the EFT can be used to extrapolate lattice results to realistic values of m_π. It was pointed out (83) that the leading (implicit as well as explicit) m_π dependence of nuclear forces can be calculated once the chiral-symmetry-breaking LEC $C_2^{(qm)}$ is known. That is because the leading m_π dependence in f_π, g_A, and m_N is known from χPT. Unfortunately, determination of $C_2^{(qm)}$ requires calculation of processes that involve external pions—e.g., πd scattering (see Section 3.4.1)—at high orders and, consequently, demands precise low-energy data. Alternatively, one can imagine fitting $C_2^{(qm)}$ to the lattice data themselves.

Note that in Figure 18, we illegally compared the EFT with quenched QCD. Most simulations cannot yet be done in QCD itself, but only in quenched or, more generally, partially quenched QCD, where different masses are assigned to valence and sea quarks. Partially quenched QCD has a different symmetry pattern than QCD, a different low-energy dynamics, and thus a different dependence on the pion mass. A proper extrapolation of partially quenched QCD data to smaller pion masses requires a partially quenched EFT. Implications of partially quenched EFT for the *NN* interaction are discussed in Reference (148).

4. OUTLOOK

4.1. More-Nucleon Systems

The EFT paradigm has been extensively applied to systems with $A = 2$–4, for momenta below and above the pion mass. Work remains to be done even for those systems, of course. For example, the chiral expansion of the pionful EFT still needs to be better understood for $A = 2, 3$; and $A = 4$ must be studied in the pionless EFT in order to uncover the role of a $4N$ force that could appear in LO.

As these issues get settled, a natural next step for the EFT program is to increase A. There have, in fact, been attempts to extend the paradigm to heavier nuclei. For example, EFT methods are being used to perfect the nuclear shell model (149).

The goal is to take some modern potential model and simplify the bound-state problem for large nuclei so as to make a numerical solution of the Schrödinger equation feasible. This simplification comes about by reducing the dimensionality of the original Hilbert space of the shell model, the effect of the highly excited states being included into local operators that act on a reduced Hilbert space. The reduced problem obtained by "integrating out" the high-energy modes can then be solved by standard numerical methods.

Another approach is to develop an EFT to handle other nuclei that are, like the deuteron, particularly lightly bound (150)—such as halo nuclei, in which the separation energy of one or more nucleons is much smaller than the energies associated with a core of the remaining nucleons.

The many EFT-inspired studies of nuclear matter ($A \to \infty$, $\alpha = 0$) and very heavy nuclei have all sought to identify the relevant degrees of freedom and an expansion parameter that can describe physics for densities near saturation (see e.g. Reference 151). Whether these approaches prove to be bona fide EFTs (in the sense used in this review) or not, the formidable problem remains of deriving the saturation of nuclear matter from an EFT adjusted to describe few-nucleon physics. The complexity of the necessary resummations of LO operators increases rapidly with A, becoming high already at $A = 5$. Lacking the identification of a further expansion parameter, we might, as in QCD itself, have to resort to lattice simulations. Müller et al. (152) have taken a step in this direction, solving a toy model with no- and two-derivative contact two-body interactions (at zero and at finite temperature) on a spatial lattice using Monte Carlo techniques, and fitting the interaction parameters to saturation properties. The next step involves using EFT interactions determined from few-nucleon systems.

4.2. Conclusion

For the past couple of years, the pionless EFT has been developed and applied to $2N$ and $3N$ systems. Although for the NN system in isolation it amounts to nothing more than effective range theory, the full power of the field-theory arsenal comes to fruition when more nucleons and/or external probes are considered. We have seen that the extension to the $3N$ system is full of surprises, such as the appearance of limit-cycle behavior and of a relevant three-body force. These surprises have been turned into successes, and relatively simple calculations yield results of quality not inferior to polished potential models. Although limited in energy, this EFT can achieve high precision for reactions of interest to astrophysics, such as $np \to d\gamma$.

The older EFT including the pion field is less well understood. There are hints that the expansion should be made around the chiral limit, but higher orders must be studied. Among the higher-order terms, one LEC, $C_2^{(qm)}$, is the main uncertainty in the extrapolation to the chiral and heavy-pion limits. External probes might be able to determine this LEC. Anyhow, considerable progress has been achieved in the development of the EFT NN potential. Isospin-violating effects are a unique virtue of the pionful EFT because they are so tightly linked to the pattern of

QCD symmetries. Issues remain regarding the size of short-range $3N$ forces, but novel longer-range $3N$ forces naturally appear and can play an important role in nuclear dynamics. Reference (153) assesses this progress from the perspective of the historical development of nuclear potentials.

Yet, most nuclei still await us.

ACKNOWLEDGMENTS

We would like to thank our collaborators for teaching us most of what we know about effective theories and nuclear physics. UvK is grateful to the Nuclear Theory Groups at the University of Washington, University of South Carolina, Ohio University, and Ohio State University, and to the Institute for Nuclear Theory for hospitality during the writing of this paper. Thanks to RIKEN, Brookhaven National Laboratory, and the U.S. Department of Energy [DE-AC02-98CH10886] for providing the facilities essential for the completion of this work. This work was supported by the Director, Office of Energy Research, Office of High Energy and Nuclear Physics, and by the Office of Basic Energy Sciences, Division of Nuclear Sciences, of the U.S. Department of Energy under Contract No. DE-AC03-76SF00098 (PFB), and by a DOE Outstanding Junior Investigator Award (UvK).

The *Annual Review of Nuclear and Particle Science* is online at http://nucl.annualreviews.org

LITERATURE CITED

1. Manohar AV. hep-ph/9606222; Kaplan DB. nucl-th/9506035; Lepage GP. In *From Actions to Answers, TASI '89*, ed. T DeGrand, D Toussaint, p. 483. Singapore: World Sci. (1990)
2. Caswell WE, Lepage GP. *Phys. Lett.* B167:437 (1986)
3. Georgi H. *Phys. Lett.* B240:447 (1990)
4. Son DT, Stephanov MA. *Phys. Rev. D* 61:074012 (2000); Beane SR, Bedaque PF, Savage MJ. *Phys. Lett.* B483:131 (2000); Barducci A, Casalbuoni R, Pettini G, Gatto R. *Phys. Rev. D* 63:074002 (2001)
5. Manohar A, Georgi H. *Nucl. Phys.* B234:189 (1984)
6. Weinberg S. *Phys. Lett.* B251:288 (1990); Weinberg S. *Nucl. Phys.* B363:3 (1991)
7. Ordóñez C, van Kolck U. *Phys. Lett.* B291:459 (1992)
8. Weinberg S. *Phys. Lett.* B295:114 (1992)
9. Ordóñez C, Ray L, van Kolck U. *Phys. Rev. Lett.* 72:1982 (1994); Ordóñez C, Ray L, van Kolck U. *Phys. Rev. C* 53:2086 (1996)
10. van Kolck U. *Phys. Rev. C* 49:2932 (1994)
11. van Kolck U. *Few-Body Syst. Suppl.* 9:444 (1995); van Kolck U. *Soft physics: applications of effective chiral Lagrangians to nuclear physics and quark models*. PhD thesis, Univ. Texas (1993)
12. Bedaque PF, van Kolck U. *Phys. Lett.* B428:221 (1998)
13. van Kolck U. In *Proc. Workshop on Chiral Dynamics 1997, Theory and Experiment*, ed. A Bernstein, D Drechsel, T Walcher, p. 62. Berlin: Springer-Verlag (1998)
14. van Kolck U. *Nucl. Phys.* A645:273 (1999)
15. Chen JW, Rupak G, Savage MJ. *Nucl. Phys.* A653:386 (1999)

16. Bethe HA. *Phys. Rev.* 76:38 (1949)
17. Efimov V. TPI-MINN-89-31-T
18. van Kolck U. *Prog. Part. Nucl. Phys.* 43:337 (1999); Beane SR, et al. In *Boris Ioffe Festschrift*, ed. M Shifman, 1:133. Singapore: World Sci. (2001)
19. Seki R, Savage MJ, van Kolck U, eds. *Nuclear Physics with Effective Field Theory*. Singapore: World Sci. (1998); Bedaque PF, Savage MJ, Seki R, van Kolck U, eds. *Nuclear Physics with Effective Field Theory II*. Singapore: World Sci. (2000)
20. Braaten E, Nieto A. hep-th/9609047; Hammer H-W, Furnstahl RJ. *Nucl. Phys.* A678:277 (2000); Furnstahl RJ, Hammer H-W, Tirfessa N. *Nucl. Phys.* A689:846 (2001); Hammer H-W, Furnstahl RJ. nucl-th/0108069
21. Bedaque PF, Hammer H-W, van Kolck U. *Phys. Rev. Lett.* 82:463 (1999); Bedaque PF, Hammer H-W, van Kolck U. *Nucl. Phys.* A646:444 (1999)
22. Bedaque PF, Braaten E, Hammer H-W. *Phys. Rev. Lett.* 85:908 (2000); Braaten E, Hammer H-W. *Phys. Rev. Lett.* 87: 160407 (2001); Braaten E, Hammer H-W, Mehen T. *Phys. Rev. Lett.* 88:040401 (2002)
23. Kaplan DB, Savage MJ, Wise MB. *Phys. Lett.* B424:390 (1998); Kaplan DB, Savage MJ, Wise MB. *Nucl. Phys.* B534:329 (1998)
24. Mehen T, Stewart IW. *Phys. Lett.* B445: 378 (1999); Gegelia J. nucl-th/9802038
25. Birse MC, McGovern JA, Richardson KG. *Phys. Lett.* B464:169 (1999)
26. Stoks VGJ, Klomp RAM, Rentmeester MCM, de Swart JJ. *Phys. Rev. C* 48:792 (1993)
27. Kong X, Ravndal F. *Phys. Lett.* B450:320 (1999); Kong X, Ravndal F. *Nucl. Phys.* A665:137 (2000)
28. Beane SR, Savage MJ. *Nucl. Phys.* A694: 511 (2001)
29. Grießhammer HW, Rupak G. *Phys. Lett.* B529:57 (2002)
30. Riska DO, Brown GE. *Phys. Lett.* B38: 193 (1972)
31. Rupak G. *Nucl. Phys.* A678:405 (2000)
32. Arenhövel H, Sanzone M. *Photodisintegration of the Deuteron: A Review of Theory and Experiment*. Berlin: Springer-Verlag (1991)
33. Chen JW, Rupak G, Savage MJ. *Phys. Lett.* B464:1 (1999)
34. Butler M, Chen JW. *Nucl. Phys.* A675:575 (2000); Butler M, Chen JW, Kong X. *Phys. Rev. C* 63:035501 (2001); Chen JW. *Nucl. Phys.* A684:484 (2001)
35. Kong X, Ravndal F. *Nucl. Phys.* A656:421 (1999); Kong X, Ravndal F. *Phys. Lett.* B470:1 (1999); Kong X, Ravndal F. *Phys. Rev. C* 64:044002 (2001); Butler M, Chen JW. *Phys. Lett.* B520:87 (2001)
36. Bedaque PF, Hammer H-W, van Kolck U. *Phys. Rev. C* 58:641 (1998)
37. Gabbiani F, Bedaque PF, Grießhammer HW. *Nucl. Phys.* A675:601 (2000)
38. Bedaque PF, Hammer H-W, van Kolck U. *Nucl. Phys.* A676:357 (2000)
39. Kaplan DB. *Nucl. Phys.* B494:471 (1997)
40. Mehen T, Stewart IW, Wise M. *Phys. Rev. Lett.* 83:931 (1999)
41. Amado RD. In *Elementary Particle Physics and Scattering Theory, Vol. 2*, ed. M Chrétien, S Schweber. New York: Gordon & Breach (1970)
42. Skorniakov GV, Ter-Martirosian KA. *Sov. Phys. JETP* 4:648 (1957)
43. van Oers WTH, Seagrave JD. *Phys. Lett.* B24:562 (1967); Phillips AC, Barton G. *Phys. Lett.* B28:378 (1969)
44. Dilg W, Koester L, Nistler W. *Phys. Lett.* B36:208 (1971)
45. Efimov VN, Tkachenko EG. JINR-E4-8473
46. Friar JL, Hüber D, Witała H, Payne GL. *Acta Phys. Polon.* B31:749 (2000)
47. Rupak G, Kong XW. nucl-th/0108059
48. Faddeev LD, Minlos RA. *Sov. Phys. JETP* 14:1315 (1962)
49. Danilov GS. *Sov. Phys. JETP* 16:1010 (1963)
50. Efimov VN. *Sov. J. Nucl. Phys.* 12:589 (1971); Efimov VN. *Sov. J. Nucl. Phys.* 28:546 (1979); Efimov VN. *Nucl. Phys.*

A210:157 (1973); Amado RD, Noble JV. *Phys. Rev. D* 5:1992 (1972)
51. Mehen T, Stewart IW, Wise MB. *Phys. Lett.* B474:145 (2000)
52. Hammer H-W, Mehen T. *Nucl. Phys.* A690:535 (2001)
53. Wilson KG. *Phys. Rev. D* 3:1818 (1971); Głazek SD, Wilson KG. *Phys. Rev. D* 47:4657 (1993)
54. Głazek SD, Wilson KG. hep-th/0203088
55. Hammer H-W, Mehen T. *Phys. Lett.* B516:353 (2001)
56. Bedaque PF, Grießhammer H, Hammer H-W, Rupak G. nucl-th/0207034
57. Kievsky A, Rosati S, Tornow W, Viviani M. *Nucl. Phys.* A607:402 (1996)
58. Phillips AC. *Nucl. Phys.* A107:209 (1968)
59. Efimov V, Tkachenko EG. *Few-Body Syst.* 4:71 (1988)
60. Efimov V, Tkachenko EG. *Phys. Lett.* B157:108 (1995)
61. Hammer H-W. nucl-th/0110031
62. Goldstone J, Salam A, Weinberg S. *Phys. Rev.* 127:965 (1962)
63. Coleman S, Wess J, Zumino B. *Phys. Rev.* 177:2239 (1969); Callan CG, Coleman S, Wess J, Zumino B. *Phys. Rev.* 177:2247 (1969)
64. Bernard V, Kaiser N, Meißner U-G. *Int. J. Mod. Phys.* E4:193 (1995)
65. Weinberg S. *Physica* 96A:327 (1979)
66. Lutz M. In hep-ph/9606301
67. Cohen TD, Hansen JM. *Phys. Lett.* B440: 233 (1998)
68. Gegelia J. nucl-th/9806028; Cohen TD, Hansen JM. *Phys. Rev. C* 59:13,304 (1999)
69. Mehen T, Stewart IW. *Phys. Lett.* B445:378 (1999); Mehen T, Stewart IW. *Phys. Rev. C* 59:2365 (1999); Mehen T, Stewart IW. *Nucl. Phys.* A665:164 (2000)
70. Steele JV, Furnstahl RJ. *Nucl. Phys.* A645: 439 (1999)
71. Rupak G, Shoresh N. *Phys. Rev. C* 60: 054004 (1999)
72. Fleming S, Mehen T, Stewart IW. *Nucl. Phys.* A677:313 (2000); Fleming S, Mehen T, Stewart IW. *Phys. Rev. C* 61: 044005 (2000)
73. Kaiser N, Brockmann R, Weise W. *Nucl. Phys.* A625:758 (1997); Kaiser N, Gerstendörfer S, Weise W. *Nucl. Phys.* A637: 395 (1998); Ballot JL, Robilotta MR, da Rocha CA. *Phys. Rev. C* 57:1574 (1998)
74. Coon SA, Friar JL. *Phys. Rev. C* 34:1060 (1986); Friar JL. *Czech. J. Phys.* 43:259 (1993)
75. Lepage GP. nucl-th/9706029; Gegelia J. *Phys. Lett.* B463:133 (1999)
76. Park T-S, Kubodera K, Min D-P, Rho M. *Phys. Rev. C* 58:637 (1998); Park T-S, Kubodera K, Min D-P, Rho M. *Nucl. Phys.* A646:83 (1999); Hyun C-H, Min D-P, Park T-S. *Phys. Lett.* B473:6 (2000)
77. Frederico T, Timóteo VS, Tomio L. *Nucl. Phys.* A653:209 (1999)
78. Epelbaum E, Glöckle W, Meißner U-G. *Nucl. Phys.* A671:295 (2000)
79. Frank WM, Land DJ, Spector RM. *Rev. Mod. Phys.* 43:36 (1971); Perelomov AM, Popov VS. *Teor. Mat. Fiz.* 4:48 (1970)
80. Beane SR, et al. *Phys. Rev. A* 64:042103 (2001)
81. Camblong HE, Ordóñez CR. hep-th/ 0110278
82. Barford T, Birse MC. nucl-th/0108024
83. Beane SR, Bedaque PF, Savage MJ, van Kolck U. *Nucl. Phys.* A700:377 (2002)
84. Sprung DWL, et al. *Phys. Rev. C* 49:2942 (1994)
85. Kaplan DB, Steele JV. *Phys. Rev. C* 60: 064002 (1999)
86. Scaldeferri KA, Phillips DR, Kao C-W, Cohen TD. *Phys. Rev. C* 56:679 (1997)
87. Gegelia J, Japaridze G. *Phys. Lett.* B517:476 (2001); Eiras D, Soto J. nucl-th/0107009
88. Lutz M. *Nucl. Phys.* A677:241 (2000)
89. Friar JL, Coon SA. *Phys. Rev. C* 49:1272 (1994); Epelbaum E, Glöckle W, Meißner U-G. *Nucl. Phys.* A637:107 (1998); Friar JL. *Phys. Rev. C* 60:034002 (1999)

90. Wiringa RB, Stoks VGJ, Schiavilla R. *Phys. Rev. C* 51:38 (1995)
91. Rentmeester MCM, Timmermans RGE, Friar JL, de Swart JJ. *Phys. Rev. Lett.* 82:4992 (1999); Timmermans RGE. Private communication (2001)
92. Epelbaum E, Meißner U-G, Glöckle W, Elster C. nucl-th/0106007
93. Kaiser N. *Phys. Rev. C* 61:014003 (2000); Kaiser N. *Phys. Rev. C* 62:024001 (2000); Kaiser N. *Phys. Rev. C* 63:044010 (2001); Kaiser N. *Phys. Rev. C* 64:057001 (2001); Kaiser N. *Phys. Rev. C* 65:017001 (2002)
94. Entem DR, Machleidt R. *Phys. Lett.* B524:93 (2002)
95. Entem DR, Machleidt R. nucl-th/0202039
96. Bogner SK, et al. nucl-th/0108041
97. Miller GA, Nefkens BMK, Slaus I. *Phys. Rep.* 194:1 (1990)
98. van Kolck U, et al. *Phys. Rev. Lett.* 80: 4386 (1998)
99. Friar JL, van Kolck U. *Phys. Rev. C* 60: 034006 (1999)
100. Niskanen JA. *Phys. Rev. C* 65:037001 (2002)
101. van Kolck U, Friar JL, Goldman T. *Phys. Lett.* B371:169 (1996)
102. Coon SA, McKellar BHJ, Stoks VGJ. *Phys. Lett.* B385:25 (1996)
103. Walzl M, Meißner U-G, Epelbaum E. *Nucl. Phys.* A693:663 (2001)
104. Epelbaum E, Meißner U-G. *Phys. Lett.* B461:287 (1999)
105. Pieper SC, Wiringa RB. *Annu. Rev. Nucl. Part. Sci.* 51:53 (2001)
106. Epelbaum E, et al. *Phys. Rev. Lett.* 86: 4787 (2001)
107. Entem DR, Machleidt R, Witała H. nucl-th/0111033
108. Coon SA, et al. *Nucl. Phys.* A317:242 (1979); Coelho HT, Das TK, Robilotta MR. *Phys. Rev. C* 28:1812 (1983)
109. Friar JL, Hüber D, van Kolck U. *Phys. Rev. C* 59:53 (1999)
110. Coon SA, Han HK. *Few-Body Syst.* 30:131 (2001); Kamada H, Hüber D, Nogga A. *Few-Body Syst.* 30:121 (2001)
111. Hüber D, et al. *Few-Body Syst.* 30:95 (2001)
112. Ellis RG, Coon SA, McKellar BHJ. *Nucl. Phys.* A438:631 (1985); Coon SA, Peña MT, Riska DO. *Phys. Rev. C* 52:2925 (1995)
113. Beane SR, Phillips DR, Malheiro M, van Kolck U. *Nucl. Phys.* A656:367 (1999)
114. Rho M. *Phys. Rev. Lett.* 66:1275 (1991)
115. Kaplan DB, Savage MJ, Wise MB. *Phys. Rev. C* 59:617 (1999); Phillips DR, Cohen TD. *Nucl. Phys.* A668:45 (2000); Walzl M, Meißner U-G. *Phys. Lett.* B513:37 (2001); Phillips DR. In *Mesons and Light Nuclei*, ed. J Adam, et al. New York: AIP (2002), in press
116. Savage MJ, Springer RP. *Nucl. Phys.* A644:235 (1998); erratum, A657:457 (1999); Savage MJ, Springer RP. *Nucl. Phys.* A686:413 (2001); Diaconescu L, Schiavilla R, van Kolck U. *Phys. Rev. C* 63:044007 (2001)
117. Park T-S, Min D-P, Rho M. *Phys. Rev. Lett.* 74:4153 (1995); *Nucl. Phys.* A596:515 (1996); Savage MJ, Scaldeferri KA, Wise MB. *Nucl. Phys.* A652:273 (1999); Park T-S, Kubodera K, Min D-P, Rho M. *Phys. Lett.* B472:232 (2000); Hyun C-H, Min D-P, Park T-S. *Phys. Lett.* B473:6 (2000)
118. Kaplan DP, Savage MJ, Springer RP, Wise MB. *Phys. Lett.* B449:1 (1999); Hyun C-H, Park T-S, Min D-P. *Phys. Lett.* B516:321 (2001)
119. Park T-S, Min D-P, Rho M. *Phys. Rep.* 233:341 (1993); Park T-S, Kubodera K, Min D-P, Rho M. *Astrophys. J.* 507:443 (1998); Park T-S, et al. nucl-th/0106025
120. Park T-S, et al. nucl-th/0107012
121. Nakamura S, et al. nucl-th/0201062
122. Ando S, Park T-S, Kubodera K, Myhrer F. nucl-th/0109053
123. Chen JW, Grießhammer HW, Savage MJ, Springer RP. *Nucl. Phys.* A644:221,245 (1998); Chen JW. *Nucl. Phys.* A653:375 (1999)
124. Beane SR, Bernard V, Lee T-SH, Meißner U-G. *Phys. Rev. C* 57:424 (1998)
125. Kaiser N. nucl-th/0203001

126. Misra A, Koltun DS. *Phys. Rev. C* 61: 024003 (2000)
127. Beane SR. hep-ph/0206219
128. Rockmore RM. *Phys. Lett.* B356:153 (1995)
129. Borasoy B, Griesshammer HW. nucl-th/ 0105048
130. Beane SR, Lee CY, van Kolck U. *Phys. Rev. C* 52:2914 (1995); Beane SR, et al. *Nucl. Phys.* A618:381 (1997)
131. Wilhelm P. *Phys. Rev. C* 56:1215 (1997)
132. Koch JH, Woloshyn RM. *Phys. Rev. C* 16:1986 (1997); Laget JM. *Phys. Rep.* 69:1 (1981)
133. Bergstrom JC, et al. *Phys. Rev. C* 57:3203 (1998)
134. Levchuk MI, Schumacher M, Wissmann F. *Nucl. Phys.* A675:621 (2000)
135. Bernard V, Krebs H, Meißner U-G. *Phys. Rev. C* 61:058201 (2000)
136. Ewald I, et al. (A1 Collab.). *Phys. Lett.* B499:238 (2001)
137. Cohen TD, Friar JL, Miller GA, van Kolck U. *Phys. Rev. C* 53:2661 (1996)
138. Hanhart C, van Kolck U, Miller GA. *Phys. Rev. Lett.* 85:2905 (2000)
139. Bernard V, Kaiser, Meißner U-G. *Eur. Phys. J. A* 4:259 (1999)
140. van Kolck U, Miller GA, Riska DO. *Phys. Lett.* B388:679 (1996); Peña MT, Riska DO, Stadler A. *Phys. Rev. C* 60:045201 (1999)
141. Park BY, et al. *Phys. Rev. C* 53:1519 (1996); Sato T, Lee T-SH, Myhrer F, Kubodera K. *Phys. Rev. C* 56:1246 (1997); Hanhart C, et al. *Phys. Lett.* B424:8 (1998); Gedalin E, Moalem A, Razdolskaya L. *Phys. Rev. C* 60:031001 (1999); Dmitrasinovic V, Kubodera K, Myhrer F, Sato T. *Phys. Lett.* B465:43 (1999); Ando S, Park T-S, Min D-P. *Phys. Lett.* B509:253 (2001)
142. da Rocha CA, Miller GA, van Kolck U. *Phys. Rev. C* 61:034613 (2000)
143. van Kolck U, Niskanen JA, Miller GA. *Phys. Lett.* B493:65 (2000)
144. Opper AK, Korkmaz E (spokespersons). TRIUMF E-704 Proposal
145. Bacher AD, Stephenson EJ (spokespersons). IUCF CE-82 Proposal
146. Hanhart C, et al. *Phys. Rev. C* 63:044002 (2001)
147. Fukugita M, et al. *Phys. Rev. D* 52:3003 (1995)
148. Beane SR, Savage MJ. hep-lat/0202013
149. Zheng DC, et al. *Phys. Rev. C* 48:1083 (1993); Haxton WC, Song CL. *Phys. Rev. Lett.* 84:5484 (2000); Haxton WC, Luu T. *Nucl. Phys.* A690:15 (2001); Fayache MS, et al. nucl-th/0112066
150. van Kolck U. In hep-ph/0201266; Bertulani CA, Hammer H-W, van Kolck U. nucl-th/0205063
151. Friar JL, Madland DG, Lynn BW. *Phys. Rev. C* 53:3085 (1996); Furnstahl RJ, Serot BD. *Nucl. Phys.* A663:513 (2000); Steele JV. nucl-th/0010066; Brown GE, Rho M. hep-ph/0103102
152. Müller H-M, Koonin SE, Seki R, van Kolck U. *Phys. Rev. C* 61:044320 (2000); Müller H-M, Seki R. See Ref. (19)
153. Machleidt R, Slaus I. *J. Phys.* G27:R69 (2001); Friar JL. *Nucl. Phys.* A684:200 (2001); Coon SA. nucl-th/9903033